Asian Journal of Chemistry; Vol. 37, No. 6 (2025), 1431-1448

ASIAN JOURNAL OF CHEMISTRY

https://doi.org/10.14233/ajchem.2025.33831

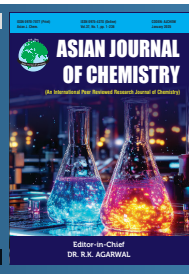

Computational and Experimental Studies on Double H-Bonded Zwitterion Dimer Model for L-2-Aminoadipic Acid

MITHIL KOTYAGOL, J. TONANNAVAR and JAYASHREE TONANNAVAR*

Vibrational Spectroscopy Group/Molecular Modelling Laboratory, Department of Physics, Karnatak University, Dharwad-580003, India

*Corresponding author: E-mail: jjtonannavar@kud.ac.in

Received: 3 April 2025; *Accepted*: 15 May 2025; *Published online*: 27 May 2025; AJC-22017

A double H-bonded zwitterion dimer structure is proposed for L-2-aminoadipic acid. The intermolecular N–H···O and O–H···O bond interactions whose vibrational modes are observed as striking IR absorption spectral features were analyzed. From molecular dynamics simulation, radial distribution function analysis showed values of 1.57 Å for the N–H···O bond and 1.68 Å for the O–H···O bond. Similarly, the radius of gyration analysis showed average values of 1.48 nm for the N–H···O bond and 1.57 nm for the O–H···O bond. DFT calculations at the B3LYP/6-311++G(d,p) level with implicit water solvation yielded the most stable zwitterion dimer. DFT results showed optimized H···O distances of 1.764 Å and 1.774 Å, with vibrational frequency redshifts of 15% (N–H···O) and 10% (O–H···O) relative to free N–H/O–H stretching frequencies. From VCD spectrum analysis, the functional groups participating in the two H-bonds exhibit non-robust modes, signifying the presence of the H-bonds in the dimer. NBO analysis shows stabilization energies of 15.5 kcal/mol (N–H···O) and 14.1 kcal/mol (O–H···O). All analyses showed that the zwitterionic structure of L-2-aminoadipic acid strengthens the N–H···O bond more than the O–H···O bond. The ECD spectra showed a broad band at 205 nm experimentally and 219 nm computationally, showing close agreement. Mole fraction variations in water reduced the intensity of the band without shifting its position. This observation has been attributed to the strong zwitterion dimer structure not amenable to dissociation into its constituent monomer species, thereby indicating that there is apparently no influence of N–H···O and O–H···O bonds on the electronic circular dichroism band structure.

Keywords: L-2-Aminoadipic acid, Molecular dynamics, N–H···O/O–H···O bonds, ECD spectrum.

INTRODUCTION

Vibrational spectroscopy combined with density functional theory (DFT) and molecular dynamics (MD) calculations has been an enriched technique for studying the wide-ranging problems including non-covalent interactions (NCI) in oligomer structures [1-4]. It is important to understand the structural and functional roles of multiple H-bonds, specifically, for example, the intermolecular N–H···O and O–H···O bonds in amino acids on account of their presence in diverse environments. However, in many instances, these H-bonds in amino acids in relation to the structural, vibrational and electronic properties are not satisfactorily investigated. For example, in a protein environment, it is important to know whether binding agents (*i.e.* amino acid as agonist or antagonist) should have proper shape or groups having favourable receptiveness to the binding site [5]. Vibrational spectroscopy aided by MD and DFT has become an enabling probe for studying dynamics, NCI and geometrical order of donor-acceptor pair in H-bonds. Further, the DFT energetics namely stabilization energy between lone pair orbital to antibonding orbital, stability of dimer energy from its two constituent monomers energies, electronic transition energies from $n \rightarrow \pi^*$ and vibrational/electronic including electronic circular dichroism (ECD) spectral properties can be correlated to the H-bonding interactions in the computed structures. In all these studies, a good agreement with experiment wherever possible is achievable. In present work, the vibrational spectroscopy combined MD/DFT was applied to characterize the N–H···O and O–H···O bonds in the most stable dimer structure of L-2-aminoadipic acid thereby achieves good agreement with the experiment.

L-2-Aminoadipic acid (α-aminoadipate, $C_6H_{11}NO_4$) is the structural analog of glutamine and L-enantiomer of 2-aminoadipic acid (Fig. 1). It is a metabolite associated with adipogenesis and is regarded as a potential biomarker of insulin resistance and obesity [6]. Its another important role is connected to the

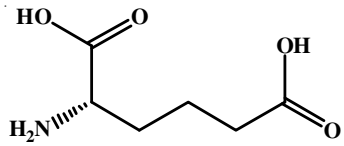

Fig. 1. Molecular structure of L-2-aminoadipic acid

dynamics of proteins especially in the involvement of making their features apparent, conformational behaviour and correlated motions. In the aging process of human skin, 2-aminoadipic acid is treated as a reliable marker for protein oxidation than its precursor allysine [7]. Single crystal XRD has shown that L-2-aminoadipic acid structure is monoclinic with space group $P2_1$ and unit cell size a = 5.136(3) Å, b = 6.992(2) Å, c = 10.065(10) Å. It is a zwitterion with the structural similarity around the amino terminus as in L-glutamic acid [5]. With two molecules of L-2-aminoadipic acid in the unit cell, they are intermolecularly bonded by N–H···O and O–H···O bonds. The NH_3^+ and COO^- groups in zwitterion L-2-aminoadipic acid produce the N–H···O bond while the two COOH groups produce the O–H···O bond. To the best of our knowledge, there have been no studies on the influence of the N–H···O and O–H···O bonds on the molecular structure including vibration and electronic properties of L-2-aminoadipic acid. The present work reports these studies for the zwitterion dimer of L-2-aminoadipic acid.

A comparative study of the N–H···O and O–H···O bonds in various ethanol ammonium-based protic ionic liquids has been reported. It has been shown that the N–H···O bond in the ion pairs is stronger than the O–H···O bond [8]. A number of studies on the N–H···O and O–H···O bonds in some of the unnatural amino acid molecular systems have been reported [9-12]. When both N–H···O and O–H···O bonds are present together in a dimer, it is of interest to evaluate their relative strengths and influence on the molecular structures and properties [13,14]. While IR absorption spectral features directly correlate to the presence of the N–H···O and O–H···O bonds, the joint presence of the two bonds defies straight-forward the spectra-structure interpretation. Furthermore, an additional layer of complexity in the vibrational and electronic structures arises in regard to their correlations to N–H···O and O–H···O bonded-dimer or higher species. The intermolecular N–H···O and O–H···O bonds arise from different donor-acceptor pairs, say, in dimer species and as a result they uniquely determine conformational states and their resultant IR spectra cannot be satisfactorily assigned owing to the unresolvable broad band contour characterized by both spectral shifts and intensity variations. Previously, we have shown that dimer, trimer, tetramer and even in some cases pentamer structures satisfactorily fit observed IR and Raman spectral features of the molecular systems in the condensed phase [15-17]. The condensed phase we mean either the sample is powder or liquid (both being the most common and crystalline phase is excluded) in which H-bonds, among other non-covalent interactions, are strong enough to cause significant IR and/or UV-visible spectral features. This has been evident in the present study, where the broad IR spectral band pattern in the region 3600-2100 cm^{-1} is apparently due to the N–H···O and O–H···O bonds and the bands are too close to be resolvable. It is in this context we combined vibrational spectroscopy with MD and DFT and computed a zwitterion dimer structure for L-2-aminoadipic acid vibrational IR and Raman modes N–H···O and O–H···O bonds arising from assuming amine salt with carboxyl salt group and carboxyl with carboxyl group, respectively. It will be shown that the most stable N–H···O (NH_3^+–COO^-)/O–H···O (COOH–COOH) bonded dimer species, among others, satisfactorily fits the experimental IR and Raman spectral features. The influence of the two H-bonds has been characterized in terms of robust and non-robust modes by performing vibrational circular dichroism (VCD) calculations. A similar influence was also studied experimentally and computationally on the electronic transition $n\rightarrow\pi^*$ at 205 nm. Mole fraction study demonstrated that the electronic circular dichroism band near 206 nm is independent of the influence of the two H-bonds.

EXPERIMENTAL

L-2-Aminoadipic acid [$HO_2C(CH_2)_3CH(NH_2)CO_2H$; ≥ 98% (TLC); m.w. = 161.16 g/mol and m.p. 203-205 ºC] was procured from Sigma-Aldrich (Merck), India and was used as received. The IR spectra of the sample in the wavenumber range of 4000-400 cm^{-1} on the Thermo-Fisher Nicolet 6700 FT-IR spectrometer were measured. The KBr pelleting technique was used for sample handling. Pellets were prepared in a sample-to-KBr ratio of 1:100. Signals were gathered at a resolution of 4 cm^{-1} for 100 scans. Raman spectra in the range 4000-50 cm^{-1} on the Bruker RFS 27 MultiRAM spectrometer were measured. It is a stand-alone interferometer bench with an Nd-YAG laser source providing the excitation wavelength of 1064 nm. Its detection system included the LN_2 cooled-Ge detector. The Raman signals were collected in the 180º geometry at a resolution of 4 cm^{-1} for 500 scans. The ECD spectrum was recorded using a JASCO-1500 Circular Dichroism Spectrophotometer in the region 190-750 nm. The spectrometer provided the Xenon arc lamp with nitrogen purging, PMT detector and double-prism monochromator. Liquid samples at concentrations 10.0-1.0 mM were prepared with water as solvent and spectra were measured using quartz cuvettes with 1 mm path length. Signals were collected at the scanning speed of 100 nm/min.

Computational details

Neutral and zwitterion monomer species: The striking IR spectra (Fig. 2) show a strong broad profile especially across the 3400-2500 cm^{-1} region characterized by a number of closely lying but unresolvable bands. Tentative assignments based on the spectra-structure correlations showed that some stretching bands due to the vibrational modes of NH_3^+ and O–H are associated with the possible intermolecular N–H···O/O–H···O bonds. Similarly, the sharper and stronger bands in the region 1605-1555 cm^{-1} arise from the bending vibrational modes due to the NH_3^+ and stretching modes of the COO^- group in addition to other bands. A band near 2086 cm^{-1} usually arises from the combination modes of a dimer [18]. These spectral evidences suggest the presence of the NH_3^+ and COO^- groups associated with L-2-aminoadipic acid being apparently a zwitterion bound by the intermolecular N–H···O/O–H···O bonds. We assumed

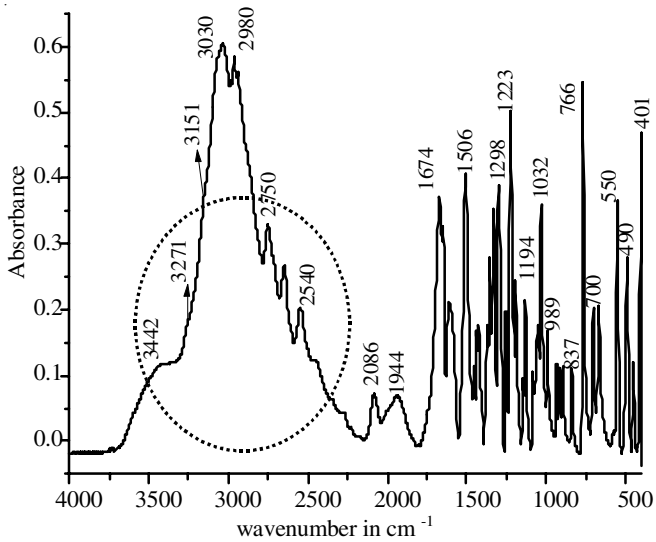

Fig. 2. FTIR spectrum of L-2-aminoadipic acid in the region of 4000-400 cm^{-1}. The broad band in functional group region 3400-2500 cm^{-1} primary indication of H-bonding represented by dotted circle

the N–H···O bond between amine salt–carboxyl salt (NH_3^+–COO^-), amine salt–carboxyl (NH_3^+–COOH) groups and O–H···O bond between carboxyl-carboxyl (COOH–COOH) and carboxyl-carboxyl salt (COOH–COO^-) groups. The first step therefore consisted of determining a stable zwitterion monomer and using this monomer to find the most stable zwitterion dimer, since the dimer is more satisfactory model for L-2-aminoadipic acid, for characterization in terms of structural, vibrational and electronic properties. To search for the most stable monomer, we defined a set of six dihedral angles (Fig. 3) and to save computational cost we ran a low-level RHF/6-31G calculation in gas phase using Gaussian 09W and Gauss View 5W suite of programs [19,20]. We obtained potential energy surfaces (PES) by varying the dihedral angles over 0º-360º at an interval of 10º (Fig. 3). The calculation finally yielded the most stable neutral monomer structure. However, the requirement was a stable zwitterion monomer, so we used SMD implicit solvation model among SCRF methods and ran optimization of the neutral monomer at B3LYP/6-311++G (d,p) level in water, finally yielding a stable zwitterion monomer (M_{ZW}, Fig. 4) [21,22]. For the purpose of MD simulation, the functional groups in M_{ZW} are conveniently referred to as backbone (B: $COO^-CHNH_3^+$) shown by dotted line and remaining structure represents side chain (S:$CH_2CH_2CH_2COOH$) as in L-glutamine [23].

Molecular dynamics simulation: The strong spectral features in favour of the zwitterion oligomer structure formed of the N–H···O and O–H···O bonds were observed previously. We used classical MD simulation to search for the most stable zwitterion

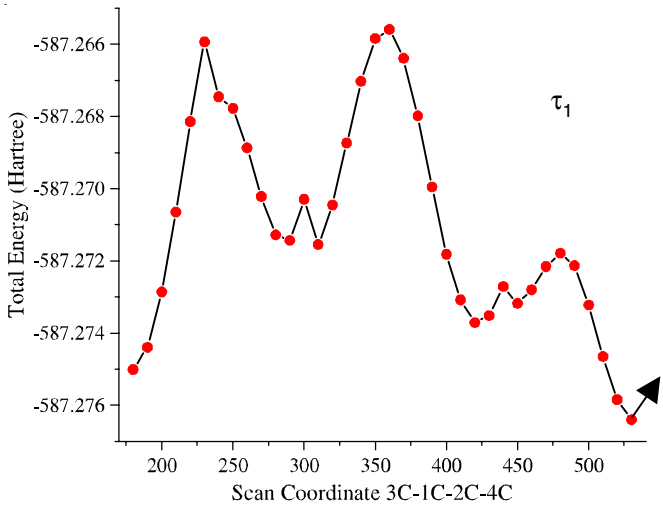

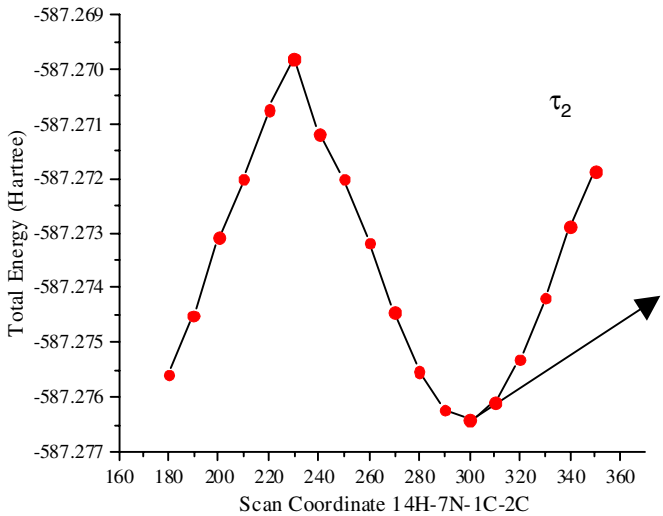

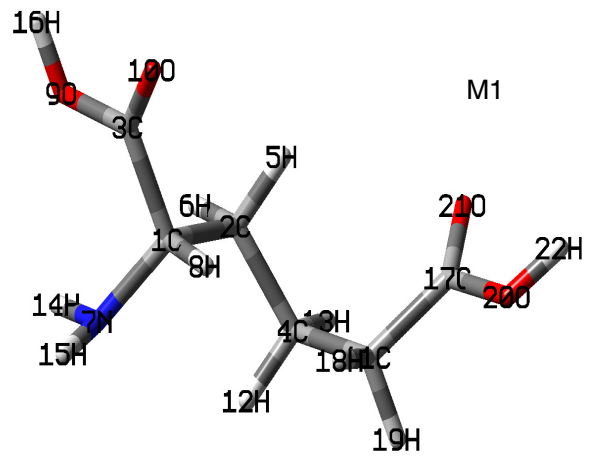

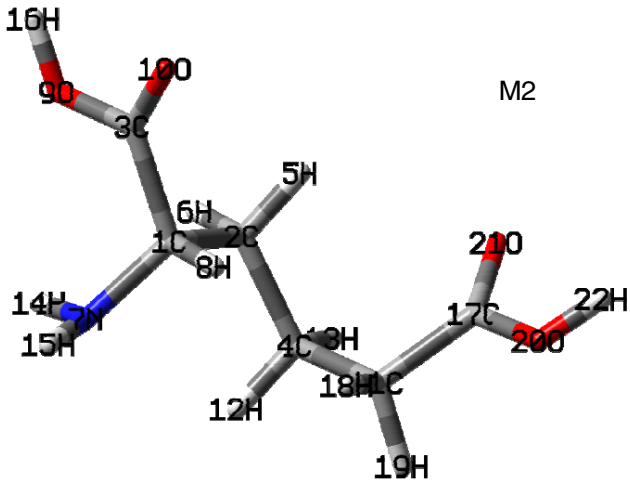

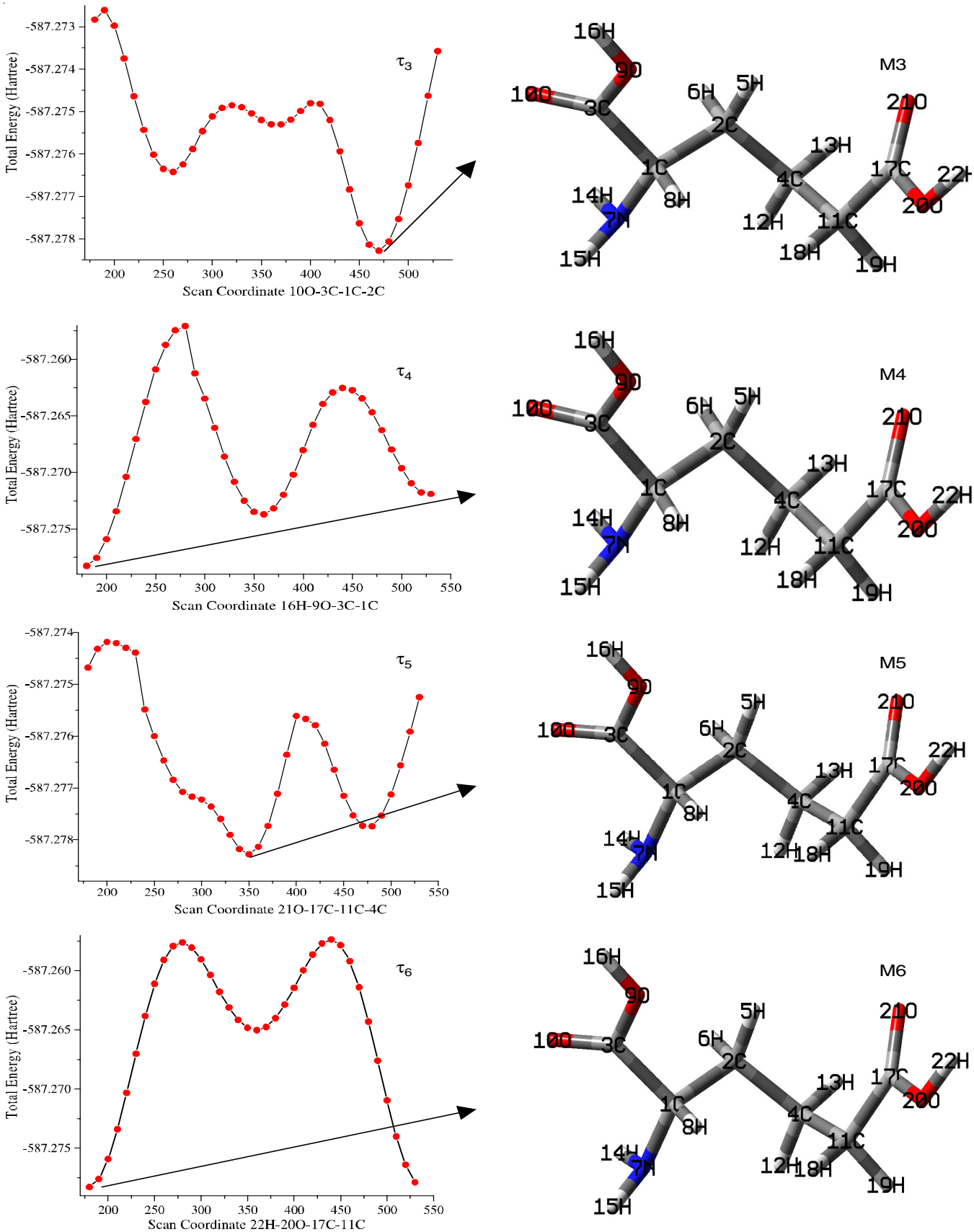

Fig. 3. PES scans (left panel) for neutral monomer structure of L-2-aminoadipic acid at RHF/6-31G in gas phase by scanning the dihedral angles τ_1 - 3C-1C-2C-4C, τ_2 - 14H-7N-1C-2C, τ_3 - 10O-3C-1C-2C, τ_4 - 16H-9O-3C-1C, τ_5 - 21O-17C-11C-4C and τ_6 - 22H-20O-17C-11C respectively over 360º (for NH_2 180º) with an interval of 10º corresponding minimum energy structures M1, M2, M3, M4, M5 and M6 (right panel) marked with arrow mark. Each scan is scanned by taking its previous step minimum energy structure

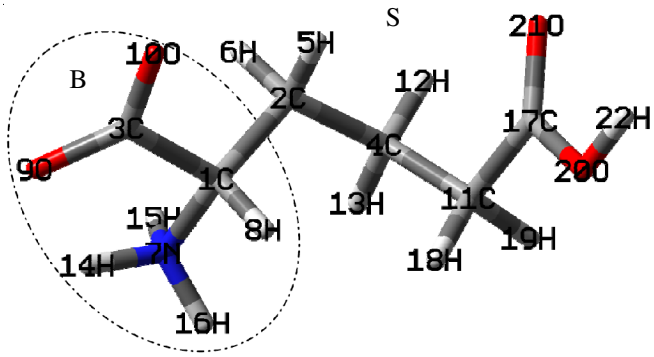

Fig. 4. Optimized zwitterionic monomer M_{ZW} structure of L-2-aminoadipic acid, computed at B3LYP/6-311++G (d, p) level with implicit solvation model with water as solvent. For our reference we divided M_{ZW} into two parts: backbone B (encircled with a dash dotted line) includes the $COO^-CHNH_3^+$ moieties and side chain S (remaining part) consists of $CH_2CH_2CH_2COOH$ moiety

dimer species formed of the N–H···O and O–H···O bonds rather than building it using DFT at B3LYP/6-311++G (d, p) level. There are two benefits from MD simulation: firstly, dimer, trimer species, *etc*. due to the N–H···O and O–H···O bonding interactions are simultaneously produced during the simulation period without the need to build them through consecutive steps using DFT; secondly, the MD simulation is less expensive. We performed the MD simulations for the M_{ZW} species using Gromacs 5.1.1 package [24-29]. For the simulation, we employed the all-atom optimal potential for liquid simulation force field. Using the CHELPG (charges from electrostatic potentials using a grid) method implemented in Gaussian 09W, we calculated partial charges for the M_{ZW} at B3LYP/6-311++G (d, p) level and borrowed Lennard-Jones parameters from the Gromacs library (Table-1) [2]. We placed ten M_{ZW} species in the triclinic box of size 2.7 × 2.4 × 2.3 nm^3 with periodic boundary conditions and 1000 water molecules. The solvation model used was transferable intermolecular potential 4P (TIP4P). We performed energy minimization on the pre-equilibrated solvent box using the steepest descent algorithm for 50,000 steps to avoid bad contacts between the solute (10 M_{ZW} species) and solvent (water) molecules. The system was further equilibrated by canonical NVT simulations and heated to the target temperature of 300 K over a duration of 100 ps. It was followed by NPT simulations at a standard atmospheric pressure of 1.0 bar with a Parrinello-Rahaman barostat for a period of 0.1 ps with V-rescale coupling to ensure a proper sampling of the canonical ensemble [30,31]. The van der Waals and electrostatic interaction cut-offs in all the simulations were set at 1.0 nm and long-range electrostatic interactions were taken into account using the particle mesh ewald technique (PME) [32]. The LINear Constraint Solver for Molecular Simulation (LINCS) algorithm, as implemented in Gromacs, was used to constrain all the covalent bonds [33]. The simulation produced oligomers ranging from dimers to nanomers (Fig. 5). The visual molecular dynamics suite (VMD) was utilized to view the different oligomeric structures with their H-bonds [34]. Fig. 6 shows eight zwitterion dimer species, which are bound either by the O–H···O or N–H···O or both bonds as a result of the interaction between the side chain (S) and backbone (B) groups. Following are the eight dimer species that were produced during the simulation: D1 [NH_3^+···COO^- & COOH···COOH (B-B & S-S)], D2 [NH_3^+···COOH & COOH···COO^- (B-S & B-S)], D3 [COOH···COOH (S-S)], D4 [NH_3^+···COO^- (B-B)], D5 [NH_3^+···COO^- & NH_3^+···COO^- (B-B & B-B)], D6 [NH_3^+···COOH (B-S)], D7 [COOH···COO^- (S-B)] and D8 [COOH···COOH & COOH···COOH (S-S & S-S)].

The N–H···O and O–H···O bonded zwitterion dimer calculations: To decide on the most stable zwitterion dimer from MD simulation output, we calculated single-point energy

TABLE-1
THE OPLS FORCE FIELDS, ESP CHARGES AND LENNARD-JONES PARAMETERS FOR THE MONOMER STRUCTURE OF L-2-AMINOADIPIC ACID

Atom types	Force field	Atoms with numbering	Electrostatic potential (ESP) charges (a.u)	van der Waals radius × 10 (nm)	Well depth × 10 (kJ mol^{-1})
CH (NH_3^+)	C(OPLS_293)	C1	-0.413230	3.50	2.7614
	H(OPLS_140)	H8	0.300684	2.50	1.2552
COO^-	C(OPLS_271)	C3	0.042437	3.75	4.3932
	O(OPLS_272)	O9	-0.570780	2.96	8.7864
		O10	-0.573450	2.96	8.7864
NH_3^+	N(OPLS_287)	N7	-0.131360	3.25	7.1128
	H(OPLS_290)	H14	0.376317	0.00	0.0000
		H15	0.351127	0.00	0.0000
		H16	0.365621	0.00	0.0000
CH_2	C(OPLS_136)	C2	-0.126720	2.96	8.7864
		C4	-0.411850	2.96	8.7864
		C11	-0.144800	2.96	8.7864
	H(OPLS_140)	H5	0.171998	2.50	1.2552
		H6	0.220945	2.50	1.2552
		H12	0.184739	2.50	1.2552
		H13	0.225489	2.50	1.2552
		H18	0.263054	2.50	1.2552
		H19	0.234408	2.50	1.2552
COOH	C(OPLS_267)	C17	-0.115700	3.75	4.3900
	O(OPLS_269)	O21	-0.393760	2.96	8.7900
	O(OPLS_268)	O20	-0.199060	3.00	7.1100
	H(OPLS_270)	H22	0.343901	0.00	0.0000

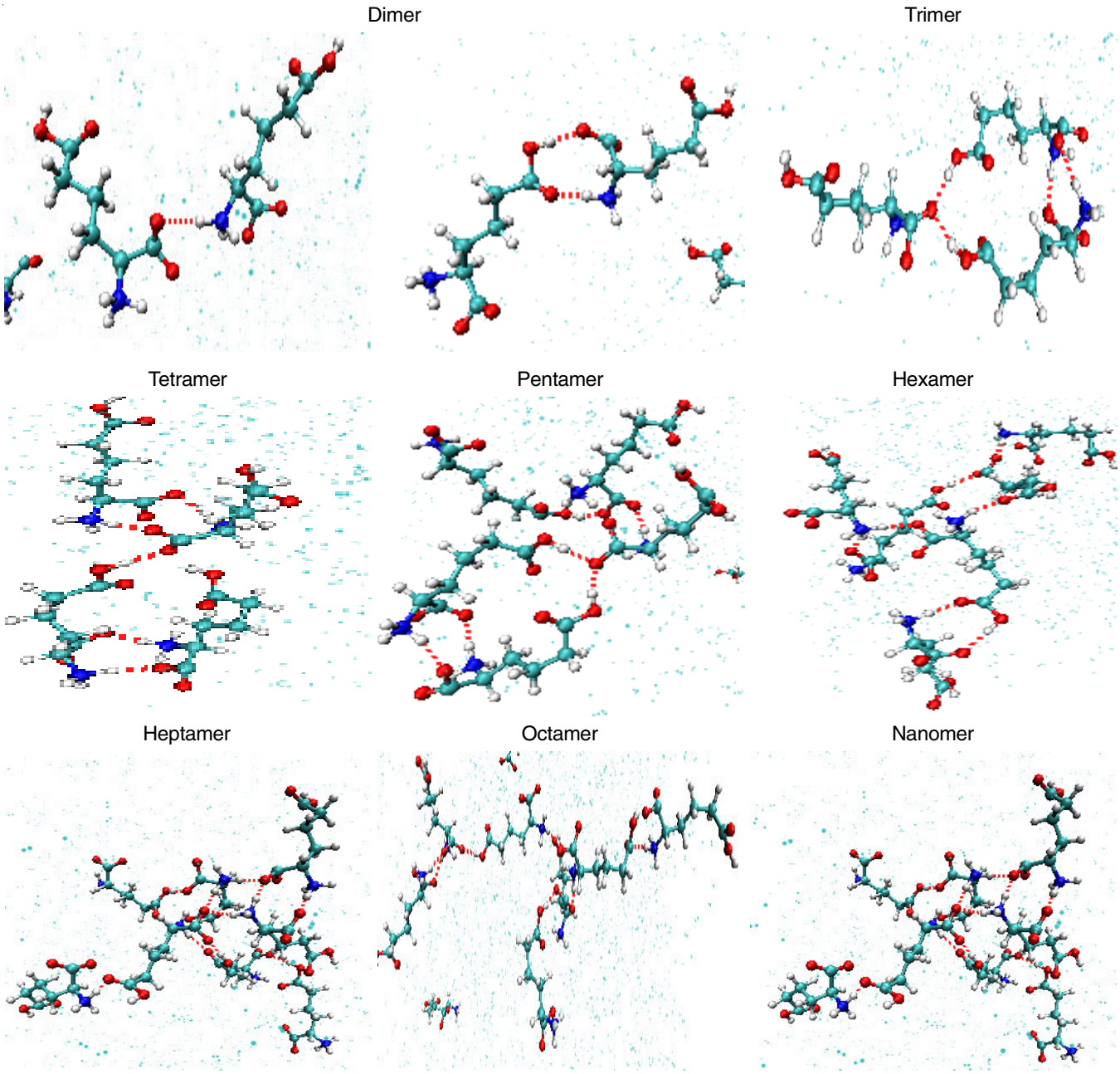

Fig. 5. Snapshot of various oligomer structures (dimer, trimer, tetramer, pentamer, hexamer, heptamer, octamer and nanomer) observed during molecular dynamics simulation of L-2-aminoadipic acid with water. L-2-aminoadipic acid molecules are shown in ball and stick style, water molecules are represented as blue dots and H-bonds between molecules are indicated by red dotted lines

for all the dimer species referred to as D1, D2, …, D8 at B3LYP/6-311++G (d,p) level. Their relative single-point energies with their Boltzmann populations are given in Table-2. From the single-point energies and Boltzmann populations of these dimer species, the D1 species were found as the most stable (Table-2). We further optimized and performed frequency calculations for D1 at B3LYP/6-311++G (d,p) level with implicit solvation using water as solvent [35]. The new zwitterion D1 dimer (D_{ZW}), is bound by N–H···O (B-B) and O–H···O (S-S) bonds lowest energy structure since it did not show any imaginary frequencies. In order to gain more insights into the N–H···O and O–H···O bonds in relation to their geometrical, vibrational, electronic and dichroic properties, we computed the MD post-processing parameters like radial distribution function, radius of gyration and DFT-natural bond orbital (NBO) and time dependent-density functional theory (TD-DFT) descriptors.

RESULTS AND DISCUSSION

Structure analysis of N–H···O and O–H···O bonded D_{ZW} dimer: A snapshot of MD production runs of the ten M_{ZW} species formed into dimers in the presence of 1000 water molecules is shown in Fig. 7. The role of water is implicit in so far as its influence is concerned. We will analyze results of the species, namely, H-bonded dimer species produced at the end of the production run. We deduced structural properties like the radial distribution functions [RDF, g(r) or alternatively it is referred

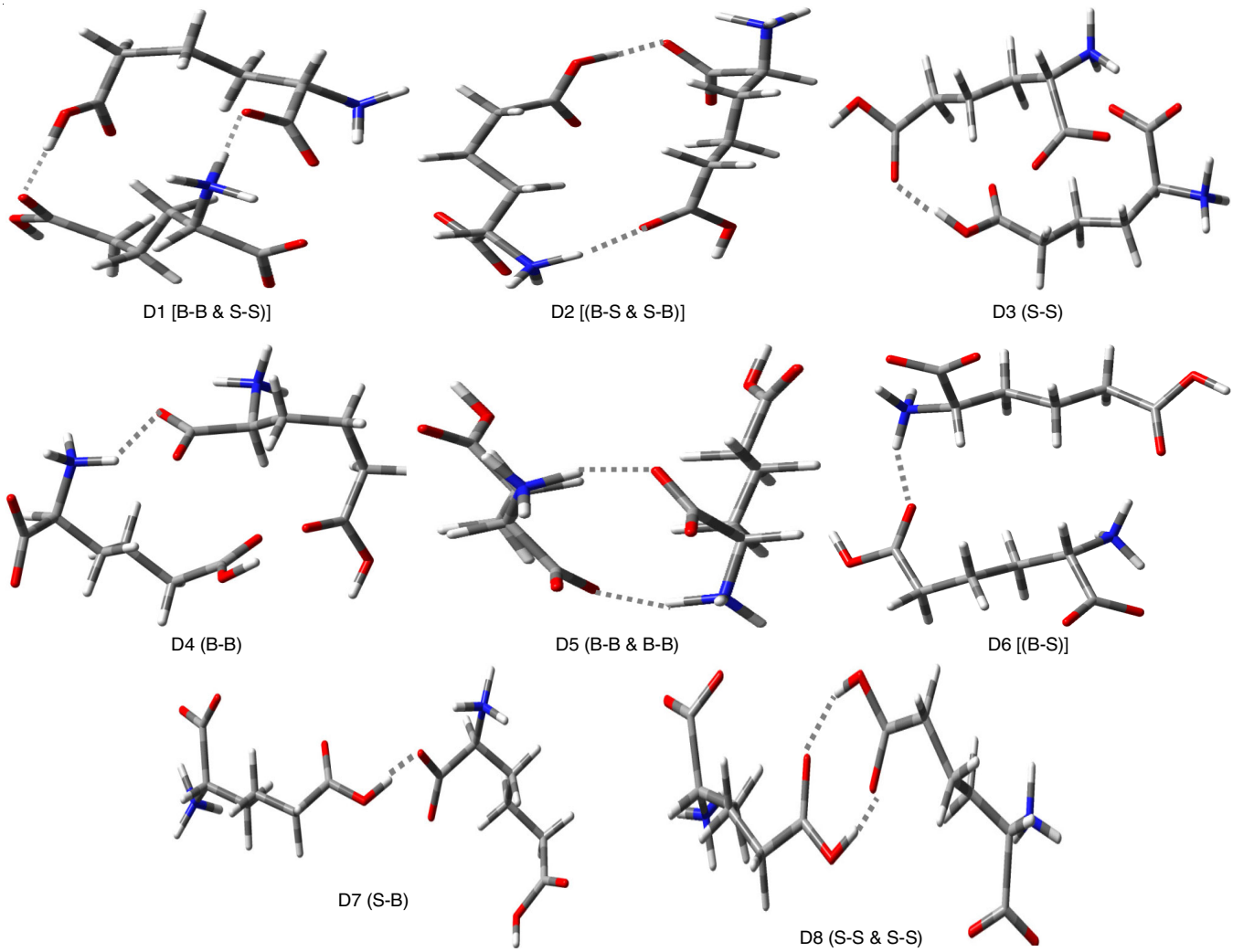

Fig. 6. Different moiety interactions showing intermolecular N–H···O and O–H···O bonded dimer structures of L-2-aminoadipic acid. These interactions include D1 [NH_3^+···COO^- & COOH···COOH (B-B & S-S)], D2 [NH_3^+···COOH & COOH···COO^- (B-S & B-S)], D3 [COOH···COOH (S-S)], D4 [NH_3^+··· COO^- (B-B)], D5 [NH_3^+···COO^- & NH_3^+···COO^- (B-B & B-B)], D6 [NH_3^+···COOH (B-S)], D7 [COOH···COO^- (S-B)] and D8 [COOH···COOH & COOH···COOH (S-S & S-S)] The labels denote the interactions between the backbone (B) and side chain (S) moieties

TABLE-2
SINGLE-POINT ENERGIES AND BOLTZMANN POPULATIONS OF H-BONDED ZWITTERION DIMERS OF L-2-AMINOADIPIC ACID CALCULATED AT THE B3LYP/6-311++G (d,p) LEVEL

Dimer (D_i)	Donor (D)	Acceptor (A)	D–H···A	Single-point energy (Hartree)	Boltzmann population (%)
D1	NH_3^+ COOH	COO^- COOH	N–H···O (B-B) O–H···O (S-S)	-1182.328682	98.0
D2	COOH NH_3^+	COO^- COOH	O–H···O (S-B) O–H···O (B-S)	-1182.324854	02.0

Note: B = Backbone, S = Side chain. The populations of the remaining dimers D3 to D8 are negligible.

to as the pair distribution function] and the radius of gyration (R_g) for the geometric characterization of the O–H···O/N–H···O bonds. The RDF refers to the chances of finding a donor atom A and an acceptor atom B [*i.e.* $g_{AB}(r)$] within some range dr of distance r from A to B. In the limit of dr→0, the fractional number of B species which fall within a thin spherical shell of volume $4\pi r^2 dr \cdot g_{AB}(r)$ surrounding the A species gives the probability distribution function [36]. It is important to observe that $g_{AB}(r)$ is measurable from X-ray, electron and neutron diffraction experiments. Further, $g_{AB}(r)$ rapidly goes to zero when $r < r_H + r_O$ where r_H and r_O are the van der Waals radii of the hydrogen (H) and oxygen (O) atoms. When r→∞, the two A and B species no longer influence each other, making $g_{AB}(r)$ independent of r and the resultant geometrical order corresponds to a homogenous medium. In this homogeneous medium, the A and B species are separable with equal probability and $g_{AB}(r) \to 1$ since they do not influence each other. With $g_{AB}(r) > 1$ indicates regions with more chances for B species to be around A; for $g_{AB}(r) < 1$, the regions have higher depletion of the B species. All the A-B distances are computed correspon-

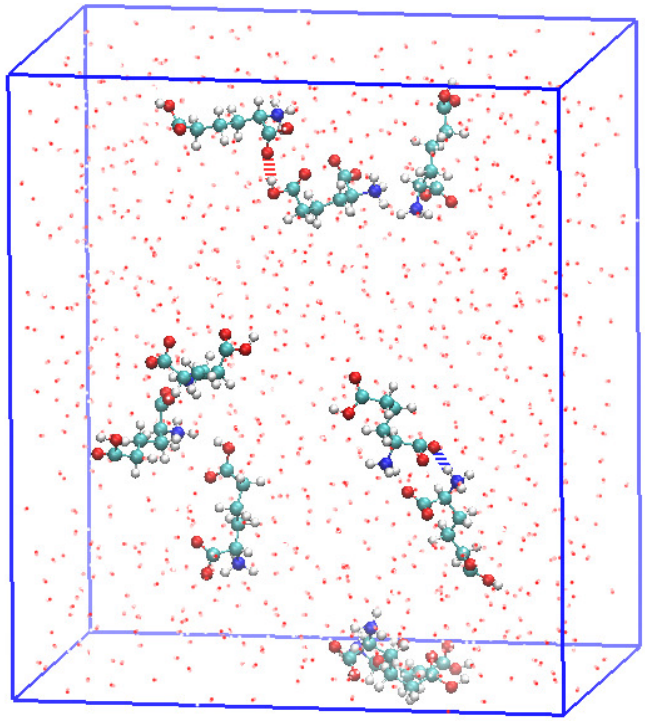

Fig. 7. Snapshot of the equilibrated simulation box containing N–H···O and O–H···O bonded dimer species formed from monomer species at 10 picoseconds along with water solvent. M_{ZW} of L-2-aminoadipic acid molecules are represented by ball-and-stick style, water molecules are represented as red dots, N–H···O (blue broken lines) and O–H···O (red broken lines) bonds

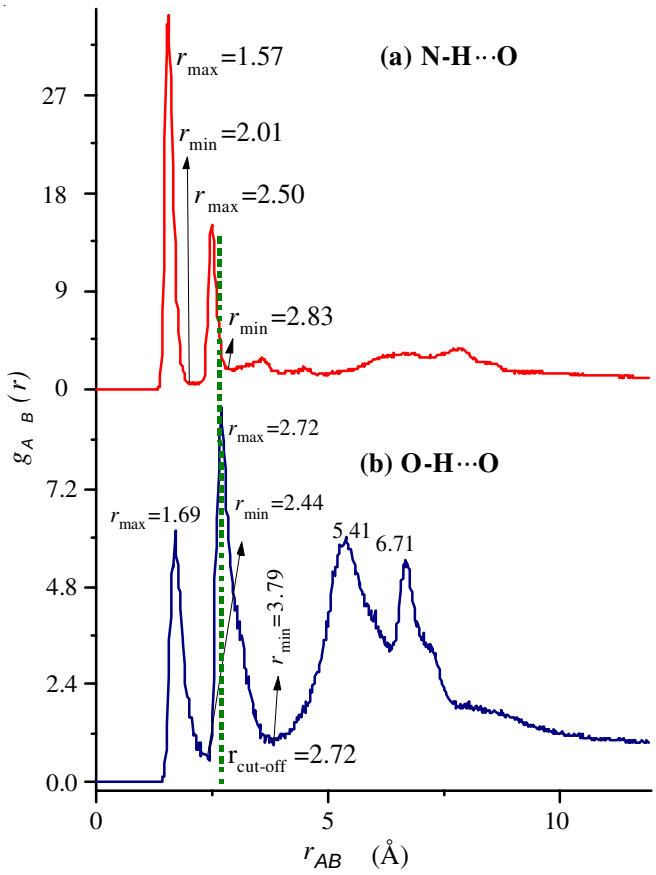

Fig. 8. Radial distribution functions (RDF) for atomic pairs donar (A) and acceptor (B) (a) N–H···O and (b) O–H···O in D_{ZW} of L-2-aminoadipic acid

ding to each snapshot of an MD simulation and each event is added to the evolution of peaks from r = 0 to r_{max} where the r_{max} being one half the simulation box. The height, width and position of the peaks in the RDF plots give a sense of geometrical order of the H-bonds [37-40]. The application of RDF to the intermolecular N–H···O and O–H···O bonds provides a different structural perspective of these H-bond interactions. If we identify the O atom as B and H atom as A in the N–H···O bond interaction and the distance $r_{H\cdots O}$ = 1.57 Å obtained from the optimization of D_{ZW} dimer being less than 2.72 Å which is the sum of the van der Waals radii r_O and r_H of O and H atoms respectively, it then follows that g_{AB} (r) rapidly decreases to zero as is seen in Fig. 8 and it corresponds to the first minimum at $r_{min} \equiv r_{H\cdots O}$ = 2.01 Å [41]. The first sharp and taller peak suggests the dominance of N–H···O bond interactions with the participation of O atoms. For larger r beyond the second peak, the g_{AB} (r) tends to approach unity suggesting its independence of r and homogeneous distribution of donor to acceptor pairs with least mutual influence. The second shorter peak suggests similar but smaller number of interactions. As for the O–H···O bond interaction, the first two sharp peaks suggest a well-defined local structure with less contribution of the H···O at r = 1.69 Å than for the second peak at r = 2.72 Å. At r = 2.72 Å, it exactly equals the sum of the van der Waals radii r_O and r_H of O and H atoms suggesting weaker interaction between the O and H atoms which is consistent with the results to be discussed later. For larger r beyond 4 Å, the broad peaks correspond to a rather homogeneous medium as has already been interpreted (Table-3). Further, the stabilization energy is 15.5 kcal/mol for the N–H···O bond and 14.1 kcal/mol for the O–H···O bond. Clearly, the N–H···O bond is stable by about 8% than the O–H···O bond. This is supported by the IR spectral shift of 15% due to the N–H···O bond with respect to the free N–H bond whereas the O–H···O bond has shown a shift of 10%. We offer the following explanation. The N–H···O bond is stronger since it is formed from the amine salt and carboxyl salt groups with strong affinity for bonding whereas the O–H···O bond is formed from the two neutral carboxyl groups.

TABLE-3
COMPARATIVE ANALYSIS OF STRUCTURAL PARAMETERS FOR N–H···O AND O–H···O H-BONDS IN MOLECULAR DYNAMICS SIMULATION OF L-2-AMINOADIPIC ACID

Bond	RDF (Å)				Avg. R_g (nm)
	1^{st} r_{max}	1^{st} r_{min}	2^{nd} r_{max}	2^{nd} r_{min}	
N–H···O	1.57	2.01	2.50	2.83	1.48
O–H···O	1.69	2.44	2.72	3.79	1.57

Note: r_{max} – maximum RDF peak, r_{min} – minimum RDF peak, Avg. R_g – average Radii of gyration (R_g).

The radius of gyration (R_g) is another parameter we computed from MD simulations, to characterize the spatial distribution of a molecular species about its center of mass. It refers to the degree to which the molecular species is compact or stretched [42,43]. The strength of the two N–H···O and O–H···O can have a direct impact on the R_g as is seen in Fig. 9. The R_g analysis shows the compression of the N–H···O and O–H···O bonds during the simulation period. The two patterns of fluctuations of R_g *versus* time are almost comparable, indicating their notable compactness during the simulation period. The R_g intervals for both H-bonds ranged from 0.69 to 2.14 nm for the N–H···O bond and 0.82 to 2.27 nm for the O–H···O bond. Further, the mean R_g value for the N–H···O bond is 1.48 nm, being lower than that of the O–H···O bond at 1.57 nm (Table-3) suggesting that the N–H···O bond exhibits more relative stability than the O–H···O bond.

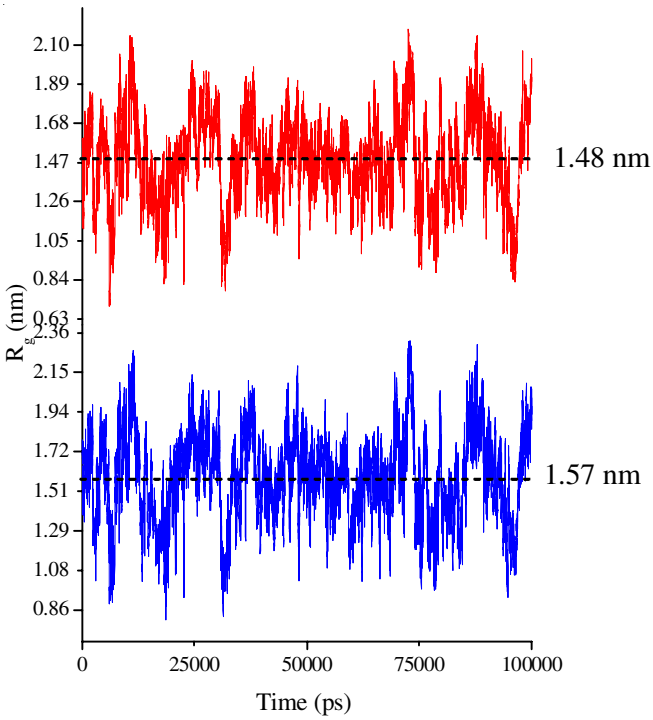

Fig. 9. The radius of gyration (R_g) of the N–H···O bond (upper) and O–H···O bond (lower) during the 100 ns MD simulation process of L-2-aminoadipic acid. Horizontal lines in both plots indicate the average R_g values (1.48 nm for N–H···O and 1.57 nm for O–H···O bond)

The optimized D_{ZW} is as shown in Fig. 10. In analyzing the structure and other properties of D_{ZW}, the M_{ZW} has served as the reference for comparing its structure and other properties. The D_{ZW} species is more stable than sum of its two constituent M_{ZW} species by ΔE = –6.49 kcal/mol (Table-4) [44]. The geometrical parameters of M_{ZW} and D_{ZW} were compared with those measured from XRD only on a nominal basis because, on the one hand, the computed values are the product of numerical results from the B3LYP/6-311++G (d, p) level; the experimental values, on the other hand, are measured for the crystalline sample which is synthesized under a set of kinetic and thermodynamic conditions. All the computed and experimental parameter values are presented in Table-5. In order to assess the

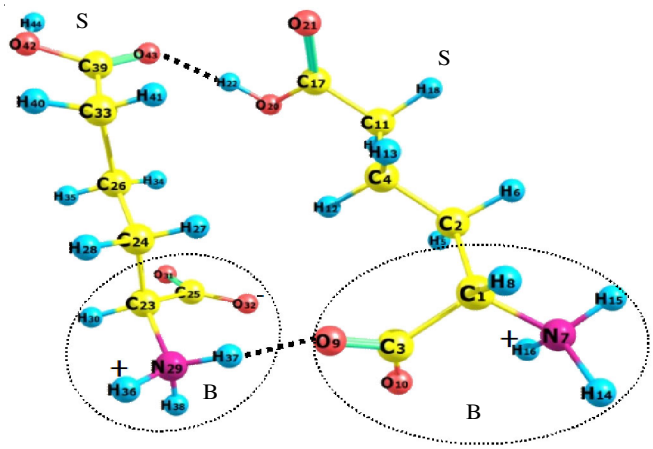

Fig. 10. Optimized double H-bonded zwitterion D_{ZW} dimer structure. (The atoms are labeled with atom numbering as used in the optimization). The backbone region (B) is encircled with dotted line and remaining part represents the side chain (S). The dotted line indicates N–H···O (B-B) and O–H···O (S-S) bonds

TABLE-4
OPTIMIZED ENERGY FOR MONOMER AND DIMER OF THE L-2-AMINOADIPIC ACID AT B3LYP/6-311++G (d, p) LEVEL

Parameter	Dimer (D_{ZW})	Monomer (M_{ZW})
Optimized energy (kcal/mol)	–741930.3797	–370961.9432

Note: $\Delta E = E_{DZW} - 2 \times E_{MZW}$ = ΔE = –741930.3797 – 2 × (–370961.9432) = –6.49 kcal/mol
$\Delta E = (E_{DZW}) - 2 \times (E_{MZW})$, where E_{DZW} refers to the energy of the optimized D_{ZW} and E_{MZW} refers to the energy of the optimized M_{ZW}.

performance of the computed parameters with respect to the XRD values, we use mean absolute deviation (MAD) and its root mean square error (RMS error) statistics [45]. As for the bond lengths, MAD values for M_{ZW} and D_{ZW} respectively are 0.011 Å and 0.010 Å and values being 0.014 Å and 0.013 Å. Similarly, for the bond angles, MAD values are 1.6º and 1.4º for M_{ZW} and D_{ZW} and RMS error values are 1.2º and 1.1º, respectively. These two sets of parameters have shown a fair agreement with the XRD results. The increase in N–H and O–H bond lengths in D_{ZW} in comparison with those in M_{ZW} is 2 to 3%. The parameters involved in the N–H···O and O–H···O bonds are evaluated separately and are presented in Table-5.

Analysis of perturbative effects of combined N–H···O/O–H···O bonds on D_{ZW} modes: There have been studies on the characterization of N–H···O and O–H···O bonds in some unnatural amino acids reported earlier [11,15,18]. Yalagi *et al.* [46] have proposed two zwitterion dimer structures, one bound by N–H···O bond and another bound by O–H···O bond for L-β-homoserine. The purpose of constructing two independent zwitterion dimer structures was to find out which one of them fitted the experimental IR and Raman spectral features [46]. Similarly, Pallavi [47] carried out a similar study for 4-hydroxy-D-phenylglycine whose dimer structures have also shown N–H···O and O–H···O bonds. Madhuri *et al.* [48] constructed a pentamer structure bound by N–H···O, O–H···O and C–H···O bonds for 5-amino-2-nitrobenzoic acid and the results are consistent with XRD structure and also in excellent agreement with near IR, IR and Raman vibrational modes. The computational analysis of electronic properties of the pentamer

TABLE-5
GEOMETRICAL PARAMETERS OF MONOMER (M_{ZW}) AND DIMER (D_{ZW}) SPECIES OF L-2-AMINOADIPIC ACID ALONG WITH EXPERIMENTAL XRD DATA

Bond lengths (Å)				Bond angles (º)			
Parameters	XRD[a]	M_{ZW}	D_{ZW}	Parameters	XRD[a]	M_{ZW}	D_{ZW}
1C-2C	1.521	1.531	1.536	1C-2C-3C	111.5	113.0	113.2
1C-3C	1.531	1.548	1.545	2C-1C-7N	108.1	110.6	108.4
1C-7N	1.496	1.507	1.506	3C-1C-7N	110.7	108.8	107.8
2C-4C	1.505	1.538	1.531	1C-2C-4C	116.8	116.0	113.5
3C-9O	1.257	1.256	1.262	1C-3C-9O	114.9	115.8	115.9
3C-10O	1.238	1.260	1.254	1C-3C-10O	117.9	117.3	117.1
4C-11C	1.496	1.532	1.543	9O-3C-10O	127.1	126.9	127.0
11C-17C	1.487	1.506	1.506	2C-4C-11C	113.5	115.5	111.3
17C-20O	1.309	1.352	1.339	4C-11C-17C	115.0	114.6	110.0
17C-21O	1.221	1.217	1.223	11C-17C-20O	115.7	112.3	113.5
				11C-17C-21O	123.3	125.8	124.0
				20O-17C-21O	121.0	121.9	122.4

H-bond distances (Å) of D_{ZW}			Bond angle (º) of D_{ZW}		
D–H···A	D–H		H···A	D–A	∠D–H···A
	M_{ZW}	D_{ZW}			
N29–H37···O9	1.02	1.05	1.764	2.814	167.9
O20–H22···O43	0.97	0.99	1.774	2.764	170.1

	Bond lengths (Å)		Bond angles (º)	
	M_{ZW}	D_{ZW}	M_{ZW}	D_{ZW}
MAD	0.011	0.010	1.6	1.4
RMS error	0.014	0.013	1.2	1.1

Note: [a]XRD values of L-2-aminoadipic acid [Ref. 5]. D = Donor (N, O), A = accepter (O). MAD = Average of difference between computed and experimental values, ignoring their sign. RMS error = root mean square error. MAD and RMS error were calculated using a method similar to the one described [Ref. 46]

has shown that the O–H···O bond is stronger than N–H···O which is in turn stronger than C–H···O. In present study, however, the proposed single dimer structure comprises N–H···O and O–H···O bonds as double bonds giving rise to its stability. In the above mentioned studies this type of double H-bond has not been reported [1,15, 46-48]. The IR spectral evidence for both zwitterion state of L-2-aminoadipic acid and the involvement of the N–H···O and O–H···O bonds in the modification of the vibrational structure (Fig. 2). Further, the two H-bonds also influence specific vibrational modes depending upon their dichroic properties. The bands at 3442, 3271 and 3151 cm^{-1} in the experimental IR spectrum are not well resolved. A broad band envelope is observed due to the presence of the N–H···O and O–H···O bonds. These broadening effects are attributed to the anharmonic vibrations and redshift in the stretching frequencies of these groups, namely, asymmetric NH_3^+ stretching, symmetric NH_3^+ stretching and symmetric OH stretching vibrations. As a result of this broadening, the individual bands are not clearly distinguishable. However, the computed D_{ZW} spectrum clearly shows these bands as sharp and resolved because the anharmonicity factor is not considered in the computational spectrum. To the best of our knowledge, previous studies have not reported this type of double H-bond in a single dimer. Therefore, we are particularly interested in studying the double H-bond in D_{ZW} of L-2-aminoadipic acid. It is of interest to see these associated changes from M_{ZW} and D_{ZW} species, which are computed for supporting the experimental vibrational structure. The experimental IR and Raman spectra are being with computed monomer M_{ZW} and D_{ZW} spectra are given in Fig. 11a-b, respectively. The IR spectrum of D_{ZW} in comparison with the experimental one shows that it is free from broad bands due to the H-bonded NH_3^+, COO^- and COOH groups across the region 3400-2500 cm^{-1}. The important bands representing H-bonding are presented in Table-6. Similarly, the experimental Raman spectrum is also free from broadband profile since Raman scattering is not sensitive to the H-bond effects. The vibrational structure of D_{ZW} is in excellent agreement with experiment demonstrating that the computed D_{ZW} is more than satisfactory to fit the experimental IR and Raman spectral features. From the spectra-structure correlations, the free OH on the COOH group has stretching frequency in the 3560–3500 cm^{-1} and it is computed at 3578 cm^{-1} and the intermolecular bonded OH stretching frequency region is 2700–2500 cm^{-1} [50-52]. We observed OH stretching frequency at 3151 and D_{ZW} band at 3196 cm^{-1}. There is a 10% redshift for OH stretching from free to bonded dimer stretching frequency. Similarly, from the spectra-structure correlations, amine salt stretching frequencies are found to be in the 3100-2600 cm^{-1}, with a broad strong band that has multiple peaks on the low-frequency wing continuing up to 2000 cm^{-1}. We observed asymmetric NH_3^+ stretching vibration at the higher frequency of 3442 cm^{-1} and a symmetric band at 3271 cm^{-1}, corresponding computed bands at 3389 cm^{-1} and 3292 cm^{-1} respectively. Due to H-bonding, we observed low frequency N-H stretching at 2863 cm^{-1} and computed at 2864 cm^{-1}. There is a 15% red shift in dimer stretching frequency from free NH_3^+ stretching at 3369 cm^{-1} to the bonded at 2864 cm^{-1}. Two medium weak distinct bands at 2086 and 1944 cm^{-1} in the experimental IR are identified as combination bands being strongly in favour of D_{ZW} [1,50]. Even low frequency bands below 200 cm^{-1} in the Raman

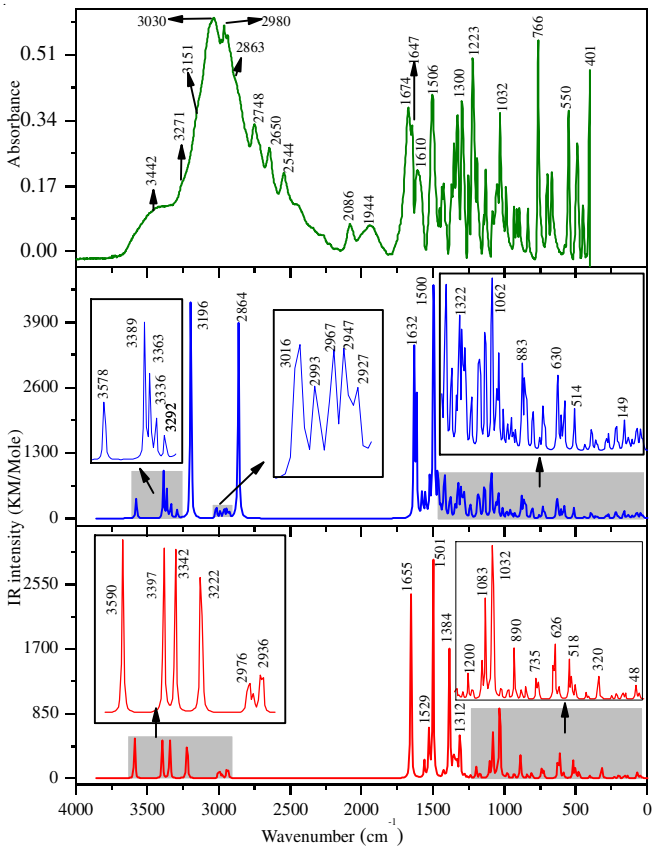

Fig. 11a. The experimental FTIR spectra (upper panel) is compared to the computed dimer D_{ZW} (middle panel) and monomer M_{ZW} (lower panel) IR spectrums of L-2-aminoadipic acid. Insets shows the enlarged images of shaded regions

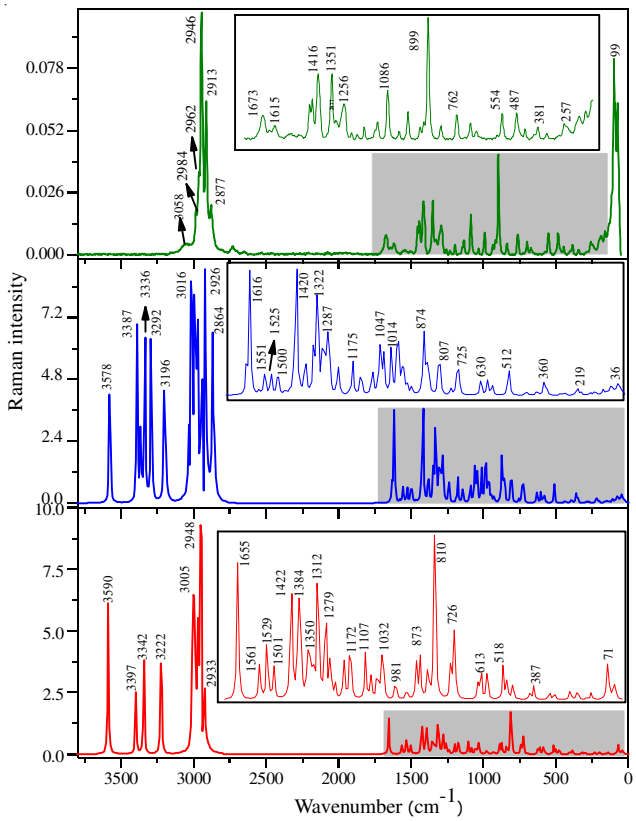

Fig. 11b. The experimental Raman spectra (upper panel) is compared to the computed dimer D_{ZW} (middle panel) and monomer M_{ZW} (lower panel) Raman spectrums of L-2-aminoadipic acid. Images of the dark areas are enlarged in the insets

spectrum, namely the strong bands at 107 and 74 cm^{-1} are accurately predicted and they describe the torsional vibrational modes of D_{ZW}. The influence of the two H-bonds have also been characterized on the basis of vibrational circular dichroic properties associated with the modes. Since L-2-aminoadipic acid is a chiral system, it should be noted that its chirality is manifested by the degree of absorption of left and right circularly polarized light radiation corresponding to the interaction between the electric dipole transition momentum (EDTM) and magnetic dipole transition momentum (MDTM). The orientation of the two transition moments EDTM and MDTM with respect to each other is a measure of the degree to which the vibrational modes are influenced by their environment giving the rotational strength (R). As a result, the vibrational modes can be grouped into robust and non-robust modes depending upon the angle ξ between EDTM and MDTM. The modes are called non-robust if the ξ of a normal mode is in the range 90° ± 30° and if the ξ is outside 90° ± 30° range are called robust modes [53-56]. Robust and non-robust modes also indicate the extent of perturbative effects associated with H-bonding as well as the degree of coupling between oscillatory and torsional vibrational motions. From Table-6, these results are shown by way of R and ξ values. It may also be noted that the robust modes are those in which the two transition moments are either nearly collinear or anti-collinear corresponding to the ξ values in the region of 60°-30° and 120°-180°, respectively. In the neighbourhood of ξ = 90° ± 5°, the contribution to R mainly comes from the EDTM with negligible contribution from the MDTM. In low frequency region, many robust modes were observed due to the combination of bending and torsional motions. Computed D_{ZW} VCD spectrum along with robust and non-robust modes is shown in Fig. 12.

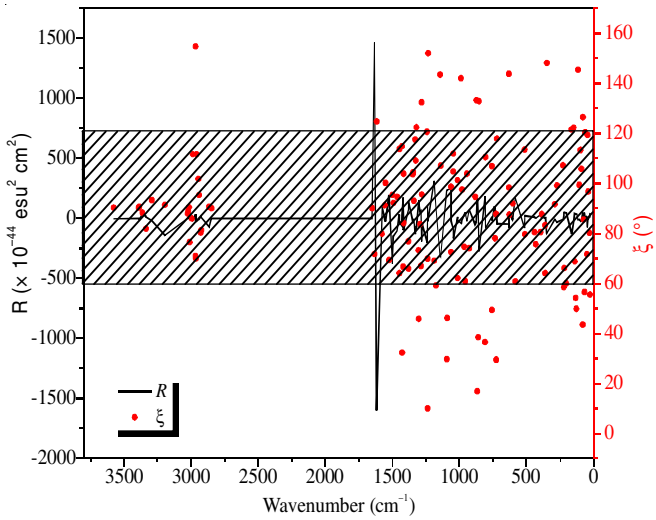

Fig. 12. Computed dimer D_{ZW} VCD spectra of L-2-aminoadipic acid. The line shows rotational strength R and dots represent angle ξ between electric and magnetic dipole transition moments of the vibrational modes in the VCD spectrum. The shaded zone denotes non-robust region angle ξ, 90° ± 30°. The remaining region represents a robust region

TABLE-6
COMPARING THE EXPERIMENTAL IR AND RAMAN VIBRATIONAL FREQUENCIES WITH THE COMPUTED MONOMER AND DIMER FREQUENCIES ALONG WITH THEIR CORRESPONDING NORMALIZED INTENSITIES, ROTATIONAL STRENGTH (R) AND THE ANGLE (ξ) BETWEEN ELECTRIC AND MAGNETIC DIPOLE TRANSITION MOMENTS OF L-2-AMINOADIPIC ACID INCLUDING ASSIGNMENTS

Wavenumber (cm^{-1})				IR intensity		Raman intensity		R	ξ	Vibrational assignments (D_{ZW})
IR	Raman	M_{ZW}	D_{ZW}	M_{ZW} × 10^{-3}	D_{ZW} × 10^{-3}	M_{ZW} × 10^{-3}	D_{ZW} × 10^{-3}	D_{ZW} × 10^{-44}	D_{ZW} (°)	
–	–	3590	3578	–	59	207	144	-4	90.28	ν OH O42-H44 free
3442w	–	3397	3389	122	42	85	78	-2	90.22	ν_{as} NH_3^+ N29-H36-H38
–	–	–	3387	–	51	–	72	-11	90.63	ν_{as} NH_3^+ N7-H14-H15-H16
–	–	–	3363	–	60	–	60	32	88.27	ν_{as} NH_3^+ N7-H14-H15-H16
–	–	3342	3336	112	35	118	177	15	81.92	ν_{s} NH_3^+ N29-H36-H38
3271m	–	3222	3292	146	22	175	187	-20	93.2	ν_{s} NH_3^+ N7-H14-H15-H16
3151s	–	–	3196	–	487	–	300	-144	91.36	ν OH O20-H22 bonded
3030vs	3058mw	–	3025	–	5	–	155	3	87.85	ν CH C1-H8
–	–	–	3022	–	12	–	57	2	88.99	ν_{as} CH_2 C33-H40-H41
–	–	–	3016	–	13	–	64	-1	90.47	ν_{as} CH_2 C11-H18-H19
–	–	3005	3011	20	3	148	129	4	76.47	ν CH C23-H30
2980vs	2984w	2997	2993	14	9	171	79	5	85.94	ν_{as} CH_2 C26-H34-H35
–	–	2991	2989	12	8	58	103	-17	111.54	ν_{as} CH_2 C4-H12-H13
–	–	2976	2967	12	8	367	187	29	70.87	ν_{s} CH_2 C33-H40-H41
–	–	–	2965	–	2	–	226	-19	**154.76**	ν_{as} CH_2 C24-H27-H28 + ν_{as} CH_2 C33-H40-H41
2962vs	2962m	–	2964	–	10	–	140	35	69.91	ν_{s} CH_2 C11-H18-H19
–	–	–	2961	–	4	–	257	-25	111.64	ν_{as} CH_2 C2-H5-H6
2938vs	2946vs	2948	2947	23	11	794	278	-14	101.84	ν_{s} CH_2 C26-H34-H
–	–	2936	2942	18	12	125	231	-8	95.28	ν_{s} CH_2 C4-H12-H13
–	2913s	2933	2927	17	10	253	399	15	80.31	ν_{s} CH_2 C24-H27-H28
–	–	–	2926	–	7	–	403	7	81.28	ν_{s} CH_2 C2-H5-H6
2863s	2877w	–	2864	–	515	–	333	-72	90.68	ν NH bonded on NH_3^+ (N–H···O) N29-H37
2086mw	–	–	–	–	–	–	–	–	--	1610 (δ_{sci} NH_3^+) + 490 (torsional NH_3^+)
1944mw	–	–	–	–	–	–	–	–	--	1506 (δ_{sci} NH_3^+) + 449 (torsional NH_3^+)
1674s	–	1655	1632	60	316	27	10	1601	**124.72**	ν CO free C17=O21 on COOH
1647m	–	–	1616	–	219	–	48	-1466	71.71	ν CO bonded C39=O43 on COOH
1610w	1673w	–	1576	–	58	–	2	95	79.87	δ_{sci} NH_3^+ N29-H36-H37-H38
–	1643mw	1561	1555	52	31	7	5	-11	91.27	δ_{sci} NH_3^+ N7-H14-H15-H16
–	1615mw	–	1551	–	24	–	6	-27	100.19	δ_{sci} NH_3^+ N29-H36-H37-H38
–	1545w	1529	1525	179	77	13	9	193	69.2	δ_{sci} NH_3^+ N7-H14-H15-H16
1506s	1505mw	1501	1500	601	351	6	5	-384	95.44	δ_{sci} NH_3^+ N7-H14-H15-H16 + ν_{as} COO^- C3-O9-O10
–	–	–	1494	–	355	–	6	-148	92.26	δ_{wag} NH_3^+ N29-H36-H37-H38 + ν_{as} COO^- C25-O31-O32
1454w	1455w	–	1466	–	135	–	1	-107	94.59	δ_{wag} NH_3^+ N29-H36-H37-H38
1439w	1441m	–	1448	–	14	–	0	30	64.11	δ_{sci} CH_2 C2-H5-H6 + δ_{sci} CH_2 C4-H12-H13 + δ_{sci} CH_2 C11-H18-H19
–	–	–	1446	–	5	–	1	-32	113.78	δ_{sci} CH_2 C24-H27-H28 + δ_{sci} CH_2 C26-H34-H35 + δ_{sci} CH_2 C33-H40-H41
–	–	–	1431	–	10	–	4	-61	114.8	δ_{sci} CH_2 C2-H5-H6 + δ_{sci} CH_2 C11-H18-H19
–	–	1428	1428	23	8	14	2	28	**32.32**	δ_{sci} CH_2 C24-H27-H28 + δ_{sci} CH_2 C33-H40-H41
1427w	–	1422	1420	8	60	14	18	175	66.67	δ_{wag} NH_3^+ N7-H14-H15-H16 + δ_{sci} CH_2 C4-H12-H13 + δ_{sci} CH_2 C11-H18-H19
–	–	–	1417	–	11	–	28	10	84.03	δ_{sci} CH_2 C24-H27-H28 + δ_{sci} CH_2 C26-H34-H35 + δ_{sci} CH_2 C33-H40-H41
–	1416s	1394	1417	33	48	22	18	-100	103.84	δ_{wag} NH_3^+ N7-H14-H15-H16 + δ_{wag} CH_2 C2-H5-H6 + δ_{wag} CH_2 C4-H12-H13 + δ_{wag} CH_2 C11-H18-H19
1371m	–	1384	1381	355	30	8	6	73	76.83	ν C23-C25 + δ C23-H30 + δ_{wag} CH_2 C24-H27-H28 + δ_{wag} CH_2 C26-H34-H35
–	–	1362	1379	36	32	1	10	144	65.92	ν C1-C3 + δ C1-H8 + δ_{wag} CH_2 C2-H5-H6 + δ_{wag} CH_2 C4-H12-H13
1356m	1351s	1350	1347	82	12	12	4	-35	103.69	δ_{sci} H22-O20-C17 + τ H19-C11-C4-H13

–	–	1343	1344	9	9	2	12	-31	104.46	τ H30-C23-C24-H27 + δ_{wag} CH_2 C26-H34-H35
–	–	–	1341	–	8	–	4	-5	93.05	δ_{sci} H22-O20-C17 + δ_{wag} CH_2 C2-H5-H6 + δ_{sci} CH_2 C4-H12-H13
1329s	1328mw	1334	1330	71	17	7	23	-133	117.56	δ C23-H30 + δ_{tws} CH_2 C24-H27-H28 + δ_{tws} CH_2 C26-H34-H35
–	–	–	1327	–	21	–	17	-116	109.08	δ C1-H8 + δ_{tws} CH_2 C2-H5-H6
–	–	–	1322	–	49	–	8	-69	122.44	δ C23-H30 + δ_{tws} CH_2 C24-H34-H35 + δ_{tws} CH_2 C26-H34-H35 + δ_{sci} CH_2 C33-H40-H41
–	–	1312	1305	184	52	32	8	102	73.19	δ H44-O42-C39 + δ_{tws} CH_2 C2-H5-H6 + δ_{tws} CH_2 C24-H34-H35 + δ_{tws} CH_2 C26-H34-H35
1300s	–	–	1303	–	27	–	16	149	**45.78**	δ H44-O42-C39 + δ H34-C26-C24
–	–	–	1293	–	22	–	7	53	83.64	δ_{wag} CH_2 C4-H12-H13 + δ H22-O20-C17 + τ H13-C4-C2-H6
–	1288w	–	1287	–	12	–	4	61	66.93	τ H41-C33-C26-C24 + τ H30-C23-C25-O32
–	–	–	1282	–	24	–	14	-190	**132.42**	δ_{tws} CH_2 C4-H12-H13 + δ_{tws} CH_2 C26-H34-H35 + δ_{tws} CH_2 C24-H34-H35
–	–	1279	1280	16	39	22	15	-45	95.47	δ_{tws} CH_2 C4-H12-H13 + δ_{tws} CH_2 C11-H18-H19
1251w	1256w	1258	1242	4	24	8	4	-202	**120.59**	δ_{tws} CH_2 C4-H12-H13 + δ_{tws} CH_2 C2-H5-H6 + δ_{tws} CH_2 C11-H18-H19 + δ H8-C1-C3
–	–	1238	1237	7	3	2	5	17	69.83	δ_{tws} CH_2 C26-H34-H35 + δ_{tws} CH_2 C24-H34-H35 + δ_{tws} CH_2 C33-H40-H41
1223vs	1231mw	–	1237	–	12	–	1	103	**10.04**	δ_{tws} CH_2 C2-H5-H6 + δ_{tws} CH_2 C11-H18-H19
–	–	–	1235	–	1	–	2	-28	**152.02**	τ H28-C24-C26-C33 + τ H41-C33-C39-O43
1194m	1196mw	1200	1187	33	79	7	1	310	69.08	ν O120-C17 + δ H22-O20-C17 + δ H18-C11-C17 + δ_{tws} CH_2 C2-H5-H6 + δ_{tws} CH_2 C11-H18-H19
1147vw	1148mw	1172	1175	20	28	13	12	97	**59.18**	δ H44-O42-C39 + δ_{tws} CH_2 C24-H34-H35 + δ_{tws} CH_2 C33-H40-H41 + δ_{tws} CH_2 C26-H34-H35
–	–	–	1143	–	31	–	4	-318	**143.41**	δ_{roc} NH_3^+ N29-H36-H37-H38 +δ_{roc} CH_2 C26-H34-H35 + δ_{roc} CH_2 C24-H34-H35 + δ_{roc} CH_2 C33-H40-H41
1134w	1133mw	–	1140	–	73	–	5	-322	107.02	δ_{roc} NH_3^+ N7-H14-H15-H16 + δ_{tws} CH_2 C4-H12-H13 + δ_{tws} CH_2 C2-H5-H6 + δ_{tws} CH_2 C11-H18-H19 + ν C17-O20 + ν C11-C14 + τ H15-N7-C1-C2
–	–	1107	1095	45	84	8	4	225	**29.67**	δ_{roc} NH_3^+ N7-H14-H15-H16 + δ H30-C23-C24 + δ_{roc} CH_2 C26-H34-H35 + δ_{roc} CH_2 C24-H34-H35 + δ_{roc} CH_2 C33-H40-H41
1086w	1086m	1083	1091	128	50	4	6	235	**46.12**	τ O20-H22···O43-C39 + τ N29-H37···O9-C3 + δ_{roc} NH_3^+ N7-H14-H15-H16 + δ_{tws} CH_2 C4-H12-H13 + δ_{tws} CH_2 C2-H5-H6 + δ_{tws} CH_2 C11-H18-H19 + δ H8-C1-C3
1055w	–	1056	1062	–	32	–	2	246	72.53	δ_{roc} NH_3^+ N29-H36-H37-H38 + τ H37-N29-C23-C24 + δ_{roc} NH_3^+ N7-H14-H15-H16 + δ_{tws} CH_2 C33-H40-H41 + ν C24-C26
–	–	–	1062	17	3	5	18	-23	98.65	δ_{roc} NH_3^+ N29-H36-H37-H38 + τ H37-N29-C23-C24 + δ_{roc} NH_3^+ N7-H14-H15-H16 + δ_{tws} CH_2 C33-H40-H41 + δ_{roc} CH_2 C26-H34-H35 + δ_{roc} CH_2 C24-H34-H35 + δ_{tws} CH_2C11-H18-H19
–	–	1038	1047	136	34	5	10	-92	104.63	τ H41-C33-C26-C24 + δ H44-O42-C39 + τ H27-C24-C23-H30 + τ C33-C26-C24-C23
1032s	1036mw	1032	1044	192	25	6	7	-169	111.87	δ H22-O20-C17
989w	992w	–	988	–	9	–	15	-43	**142.04**	δ H30-C23-C24
–	–	979	981	23	10	4	14	-17	97.56	τ C11-C4-C2-C1
–	–	–	958	–	16	–	7	47	60.88	ν N29-C23 + ν C23-C24 + τ N29-C23-C24-C26 + τ H36-N29-C23-H30 + τ H40-C33-C26-H34
935w	934mw	–	944	–	7	–	3	-28	103.84	δ C24-C26-C33 + τ H30-C23-C24-H27
918w	917mw	932	926	20	11	2	3	73	74.06	τ H14-N7-C1-C2 + τ C1-C2-C4-C11
897w	899vs	890	883	65	47	6	3	-53	94.72	δ O20-H22 + τ H22-O20-C17-C11
–	–	–	867	–	29	–	4	171	**16.76**	δ O20-H22 + ν C17-O20 + τ H22-O20-C17-C11
835w	838mw	841	854	16	43	6	10	-274	**132.77**	δ O20-H22 + ν C17-O20 + τ H22-O20-C17-C11
–	–	–	807	–	14	–	2	-80	110.41	δ H30-C23-C25
766vs	–	740	735	33	20	6	6	99	77.99	τ H22-O20-C17-O21 + τ C17-C11-C4-C2 + τ H19-C11-C4-H12

–	–	–	725	–	2	–	8	19	**29.44**	τ H22-O20-C17-C11 + τ H19-C11-C4-C2
671w	676mw	–	633	–	3	–	3	-48	**143.81**	τ H37···O9-C3-C1 + τ H15-N7-C1-C2
–	–	–	631	–	27	–	2	-83	98.25	τ C23-N29-H37···O9 + τ H44-O42-C39-C33
–	–	626	630	36	39	2	2	41	87.45	τ H44-O42-C39-O43 + τ H30-C23-N29-H37
–	–	613	603	87	16	5	4	-9	91.93	τ H22-O20-C17-O21+ τ H22-O20-C17-C11
550s	554m	586	583	18	35	5	4	171	60.79	τ H44-O42-C39-O43 + τ H44-O42-C39-C33
–	–	518	514	49	21	5	5	-82	113.52	τ O9-C3-C1-C2 + τ N7-C1-C2-C4 + τ N29-H37···O9-C3
490m	487m	501	512	29	9	3	4	19	79.5	τ O31-C25-C23-H30 + τ N29-C23-C24-C26
449w	444mw	477	440	28	3	3	1	12	80.42	δ O21-C17-C11 + τ H18-C11-C17-O21 + τ H22-O20-C17-C11
401s	–	404	431	11	2	1	1	2	75.59	τ H44-O42-C39-O43
–	–	–	395	–	10	–	1	29	80.51	τ N29-C23-C24-C26
–	381mw	387	386	3	7	2	1	6	87.83	τ N29-H37···O9-C3 + τ N7-C1-C2-C4
–	–	–	362	–	5	–	3	5	83.21	τ H44-O42-C39-C33
–	–	–	360	–	1	–	1	14	64.08	τ C1-C2-C4-C11
–	–	320	350	7	3	1	2	-123	**148.19**	τ N29-C23-C24-C26
–	–	297	289	2	9	1	1	-7	91.57	τ N7-C1-C3-O10
–	–	–	273	–	10	–	1	-33	99.15	τ N29-C23-C24-C25
–	257mw	230	227	6	5	1	0	-11	107.25	τ N29-H37···O9-C3 + τ N7-C1-C2-C4 + τ O20-H22···O43-C39
–	–	–	220	–	12	–	1	23	**58.39**	τ N29-H37···O9-C3 + τ N7-C1-C2-C4 + τ O20-H22···O43-C39 + τ C1-C2-C4-C11 + τ C23-C24-C26-C33
–	–	–	219	–	6	–	1	51	66.12	τ N29-H37···O9-C3 + τ O20-H22···O43-C39 + τ C1-C2-C4-C11 + τ C23-C24-C26-C33
–	188w	198	204	12	5	2	1	46	**59.93**	τ O20-H22···O43-C39 + τ C1-C2-C4-C11 + τ C23-C24-C26-C33
–	–	158	164	12	18	0	1	-131	**121.42**	τ N29-H37···O9-C3 + τ O20-H22···O43-C39 + τ N7-C1-C2-C4 + τ N29-C23-C24-C25 + τ C1-C2-C4-C11
–	–	139	149	8	2	1	1	-41	**122.32**	τ O20-H22···O43-C39 + τ N7-C1-C2-H6 + τ C1-C2-C4-C11
–	–	–	141	–	2	–	0	42	68.74	τ O20-H22···O43-C39 + τ H14-N7-C1-C2-H8 + τ C1-C2-C4-C11
–	–	–	134	–	6	–	0	38	**54.24**	τ C23-C24-C26-C33 + τ H44-O42-C39-C26
–	–	–	127	–	4	–	0	35	**49.76**	τ C23-C24-C26-C33 + τ N29-H37···O9-C3 + τ O20-H22···O43-C39 + τ C1-C2-C4-C11
–	–	–	117	–	0	–	0	-13	**145.44**	τ O20-H22···O43-C39 + τ H44-O42-C39-C33 + τ O21-C17-C11-C4 + τ C1-C2-C4-C11
–	107m	–	108	–	5	–	1	-8	99.33	τ N29-H37···O9-C3 + τ O20-H22···O43-C39 + τ N29-C23-C24-C25 + τ C1-C2-C4-C11
–	99vs	–	97	–	3	–	1	-24	113.38	τ O20-H22···O43-C39 + τ H44-O42-C39-O43
—	–	–	90	–	1	–	1	-5	105.71	τ C1-C2-C4-C11 + τ C23-C24-C26-C33
–	–	–	82	–	6	–	–	50	**43.51**	τ C23-C24-C26-C33 + τ N29-H37···O9-C3 + τ O20-H22···O43-C39 + τ C1-C2-C4-C11
–	–	–	80	–	–	–	1	-6	**126.45**	τ O20-H22···O43-C39 + τ H44-O42-C39-C33 + τ O21-C17-C11-C4 + τ C1-C2-C4-C11
-	74s	71	74	13	9	2	1	11	85.49	τ N29-H37···O9-C3 + τ O20-H22···O43-C39 + τ O10-C3-C1-N7 + τ O31-C25-C23-N29 + τ H44-O42-C39-O43 + τ O21-C17-C11-C4
–	–	67	68	9	7	4	1	48	**56.43**	τ N29-H37···O9-C3 +τ O20-H22···O43-C39 + τ N29-C23-C24-C26 +τ H44-O42-C39-C33 + τ O21-C17-C11-C4
–	–	–	63	–	5	–	1	-13	**120.31**	τ N29-H37···O9-C3 + τ O20-H22···O43-C39 + τ H19-C11-C4-H18 + τ H12-C4-H13-C2 + τ O21-C17-C11-C4
–	–	–	50	–	3	–	2	20	71.64	τ N29-H37···O9-C3 + τ O20-H22···O43-C39 + τ O31-C25-C23-C24 + τ O21-C17-C11-C4 + τ O32-C25-C23-C29
–	–	48	46	9	7	1	1	-75	119.3	τ N29-H37···O9-C3 + τ O20-H22···O43-C39 + τ O32-C25-C23-C29 + τ H16-N7-C1-C2

–	–	–	41	–	5	–	2	-8	96.67	τ N29-H37···O9-C3 + τ O20-H22···O43-C39 + τ O32-C25-C23-C29 + τ H16-N7-C1-C2 + τ H44-O42-C39-C33
–	–	36	30	3	3	2	1	9	80.15	τ N29-H37···O9-C3 + τ O20-H22···O43-C39 + τ O32-C25-C23-O31 + τ H16-N7-C1-C2 + τ H44-O42-C39-C33 + τ O10-C3-C1-C2 + τ O21-C17-C11-C4
–	–	–	26	–	3	–	1	41	**55.5**	τ N29-H37···O9-C3 + τ O20-H22···O43-C39 + τ O32-C25-C23-O31 + τ N7-C1-C2-C4 + τ H38-N29-C23-C33 + τ O10-C3-C1-C2 + τ O21-C17-C11-C24 + τ H44-O42-C39-C33

Note: M_{ZW} - Monomer, D_{ZW} - Dimer, R - Rotational strength, and ξ - E-M angle. Computed frequencies are scaled by 0.9668 scaling factor [Ref. 49]. Intensities of experimental bands are described as: vs = very strong s = strong. m = medium. w = weak. mw = medium weak. Mode description: ν_s = symmetric stretching, ν_{as} = asymmetric stretching, δ = bending, τ = torsional. Computed frequency in cm^{-1}, Intensity are shown in this table are normalized, IR intensity in KM/mole, Raman intensity in $Å^4$/a.m.u, R in 10^{-44} esu^2 cm^2 and the robust modes ξ values are given in bold.

Electronic structure analysis of D_{ZW}: To ascertain the degree of overlap of the associated molecular orbitals of the donors and acceptors in the O–H···O and N–H···O bonding interactions, we performed natural bond orbital (NBO) analysis at B3LYP/6-311++G (d, p) level. A stabilizing donor-acceptor interaction is characterized by electron density delocalization between occupied Lewis-type (bonding or lone pair orbitals) NBOs and vacant non-Lewis NBOs (anti-bonding orbitals) [57,58]. The orbital overlap between the antibonding orbital (σ*) of the donors, N–H and O–H and that of lone pair orbital LP(n) of the acceptor O atom, LP(n)→σ*, yielded stabilization energy $E^{(2)}$ values of 15.5 and 14.1 kcal/mol for the N–H···O and O–H···O bonding interactions, respectively. We present electron density maps of the NBOs involved in these interactions in Fig. 13.

In ECD, there is differential absorption of the left and right handed circularly polarized components of the incident light by the molecule. As a result, the electronic transition is associated with the electric vector of the incident light and the molecular electronic transition moment resulting in the interaction between the two which corresponds to the observed ECD spectrum [59,60]. Since L-2-aminoadipic acid is chiral, we measured

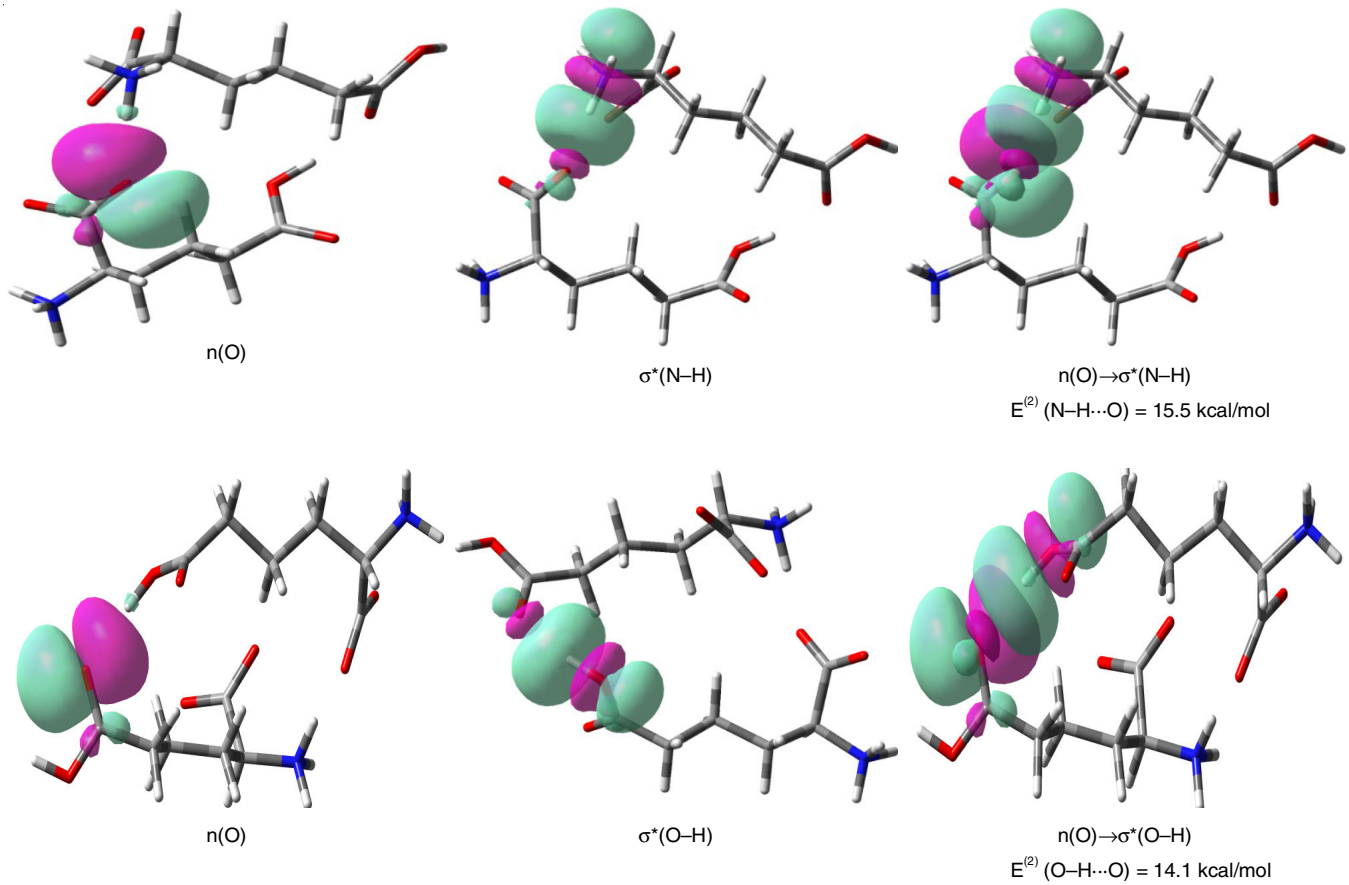

Fig 13. Electron density maps of overlapping n(O)→σ*(O–H/N–H) NBOs due to N–H···O (upper panel) and O–H···O (lower panel) bonding at B3LYP/6-311++G (d,p) level in D_{ZW} of L-2-aminoadipic acid

its ECD spectra in water in the 190-750 nm. There is a strong and broad absorption at 205 nm (~ 6.05 eV) with FWHM of Δλ ~ 25 nm (ΔE = 1.36 eV), which remain steady even for decrease in concentrations from 10.0 to 1.0 mM (Fig. 14) [61]. It is noteworthy that the absorption strength diminishes from 10 to 1 mM by a factor of 12, while the peak position remains unchanged in wavelength [15]. To understand the mechanism, we computed ECD spectrum using TD-DFT method at CAM-B3LYP/6-31G level with implicit solvation in water (Fig. 14) [62]. It yielded a band value of at 219 nm (~5.66 eV) due to the transition $^1A \leftarrow {}^1X$ (where X = singlet ground state and A = singlet first excited state) in fair agreement with the experimental value within 7% [63,64]. There is the electronic transition from HOMO n(COO^-) →LUMO π*(C=O on COOH) groups. The HOMO and LUMO energy gap is estimated to be 6.42 eV (Fig. 15).

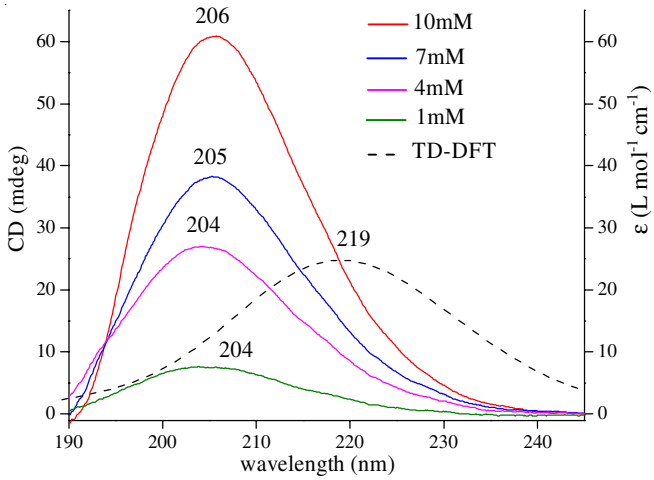

Fig. 14. Comparison of experimental ECD spectra of L-2-aminoadipic acid at different concentrations (10, 7, 4, 1 mM in water) represented by solid lines and computed ECD spectrum of dimer D_{ZW} at TD-DFT CAM-B3LYP/6-31G level represented by dashed line. (Left vertical scale corresponds to experimental ECD spectrum measured in CD and right vertical scale corresponds to computed ECD spectrum in differential extinction coefficient Δε)

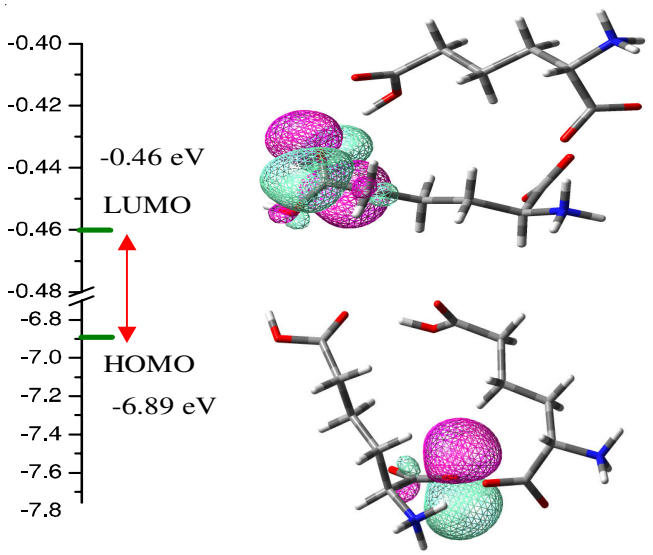

Fig. 15. Highest occupied molecular orbital (HOMO) and lowest unoccupied molecular orbital (LUMO) energy gap for the zwitterionic dimer (D_{ZW}) of L-2-aminoadipic acid

From the NBO analysis, we affirm that the electron delocalizations are: n(O9)→σ*(N29–H37) in NH_3^+ corresponding to the N29–H37···O9 bonding and n(O43)→σ*(O20–H22) in COOH corresponding to the O20–H22···O43 bonding. We have seen above a single broad band at 205 nm does not shift even for concentration variations on the longer wavelength side suggesting that there is apparently no closely-lying transition caused by the presence of individual M_{ZW} species from the dissociation of D_{ZW} species in water. The tentative explanation is that the energies associated with the N–H···O and O–H···O bonding interactions are 0.67eV (~15.5 kcal/mol) and 0.61 eV (~14.1 kcal/mol), being small enough in comparison with the electronic transition energies in the neighborhood of 5.6 eV and therefore the influence of two H-bonds on the electronic structure of L-2-aminoadipic acid is not apparent. Another factor we wish to discuss is as follows: the broadband envelope at 205 nm, as a rule, is the result of simultaneous electronic and vibrational transitions (rotational transitions are too weak) and IR spectrum (Figs. 2 and 11a) being rich with closely-lying bands suggesting a number of vibrational transitions being excited during the electronic transition, $^1A \leftarrow {}^1X$. It is possible that there is vibrational relaxation which is non-radiative process induced in the solvent medium with typical time scale in the domain of a few picoseconds, being smaller than the vibrational time periods, resulting in the broad band with no vibrational structure. If we assume further that the vibrational modes of the two N–H···O and O–H···O bonds are part of the vibrational relaxation accompanied by large anharmonicities giving rise to the electronic band as above at 205 nm as structureless. This explanation is consistent with this observation.

Conclusion

From the experimental IR spectrum, a strong broad band near 3400-2600 cm^{-1}, a combination band near 2000 cm^{-1} and the reported XRD structure provide primary evidence for the zwitterionic state and intermolecular N–H···O and O–H···O bonding in the dimer species of L-2-aminoadipic acid. During molecular dynamics simulation, different oligomer structures were observed. The radial distribution function analysis revealed first r_{max} values of 1.57 Å for the N–H···O bond and 1.69 Å for the O–H···O bond, indicating that the N–H···O bond is stronger than the O–H···O bond. Similarly, the radius of gyration (R_g) analysis showed average values of 1.48 nm for the N–H···O bond and 1.57 nm for the O–H···O bond, suggesting greater stability for the N–H···O bond. Among all possible dimer and higher-order species, the proposed double-H-bonded zwitterion dimer was found to have the lowest energy structure at the B3LYP/6-311++G(d,p) level with implicit water solvation. The dimer formation is attributed to the two intermolecular N–H···O and O–H···O bonds, consistent with the reported XRD structure. Striking IR absorption features correlated to functional groups NH_3^+, COO^- and COOH. The vibrational modes of the dimer are in excellent agreement with IR and Raman bands. The optimized H···O bond lengths, as determined by a DFT study, were 1.764 Å and 1.774 Å. These bond distances are associated with redshifts in the stretching vibrational frequencies by 15% for N–H···O bonds and 10% for O–H···O bonds,

respectively. The computed vibrational circular dichroism spectrum showed that the functional groups involved in the two H-bonds exhibit non-robust modes, confirming the presence of the two H-bonds in the dimer. NBO analysis indicated electron delocalization between lone-pair orbitals and antibonding orbitals, providing stabilization energy values of 15.5 kcal/mol for the N–H···O bond and 14.1 kcal/mol for the O–H···O bond. The broad electronic circular dichroism (ECD) band observed at 205 nm, attributed to the electronic transition $^1A \rightarrow {}^1X$, was computed at 219 nm using the TD-DFT method. Concentration-dependent ECD spectra analysis showed no wavelength shift at 205 nm, indicating that the dimer does not dissociate into its constituent monomer species. The ECD band has not shown any shift due to the N–H···O and O–H···O bonds on the electronic structure of L-2-aminoadipic acid since their stabilization energies are too small compared to the electronic transition energy.

ACKNOWLEDGEMENTS

The authors thank the Director, USIC, Karnatak University, Dharwad, India for FT-IR, FT-Raman and ECD spectral analysis. One of the authors, MK, gratefully acknowledges the Ministry of Tribal Affairs, Government of India, for awarding fellowship under the National Fellowship for ST students. Thanks are also due Prof. S. Umapathy for a visit to his MD computational lab (Department of IPC, Indian Institute of Science, Bengaluru) by Prof. Jayashree Tonannavar.

CONFLICT OF INTEREST

The authors declare that there is no conflict of interests regarding the publication of this article.

REFERENCES

1. L. Pallavi, J. Tonannavar and J. Tonannavar, *J. Mol. Liq.*, **352**, 118746 (2022); https://doi.org/10.1016/j.molliq.2022.118746
2. J. Bhovi, J. Tonannavar and J. Tonannavar, *J. Mol. Struct.*, **1299**, 137077 (2024); https://doi.org/10.1016/j.molstruc.2023.137077
3. A. Jezierska, J.J. Panek, G.Z. Zukowska and A. Sporzyñski, *J. Phys. Org. Chem.*, **23**, 451 (2010); https://doi.org/10.1002/poc.1625
4. Z. Dezhahang, M.R. Poopari and Y. Xu, *J. Mol. Struct.*, **1024**, 123 (2012); https://doi.org/10.1016/j.molstruc.2012.04.079
5. J.N. Low, R.A. Howie, C.M. Scrimgeour and P.W. Watt, *Acta Crystallogr. C*, **44**, 1762 (1988); https://doi.org/10.1107/S0108270188006997
6. H.J. Lee, H.B. Jang, W.-H. Kim, K.J. Park, K.Y. Kim, S.I. Park and H.-J. Lee, *Sci. Rep.*, **9**, 13610 (2019); https://doi.org/10.1038/s41598-019-49578-z
7. R.D. Sell, C.M. Strauch, W. Shen and V.M. Monnier, *Biochem. J.*, **404**, 269 (2007); https://doi.org/10.1042/BJ20061645
8. I.V. Fedorova and L.P. Safonova, *Struct. Chem.*, **32**, 2061 (2021); https://doi.org/10.1007/s11224-021-01792-0
9. R.P. Kavali, J. Tonannavar, J. Bhovi and J. Tonannavar, *J. Mol. Struct.*, **1264**, 133174 (2022); https://doi.org/10.1016/j.molstruc.2022.133174
10. S.S. Malaganvi, J. Tonannavar (Yenagi) and J. Tonannavar, *Heliyon*, **5**, (2019); https://doi.org/10.1016/j.heliyon.2019.e01586
11. S. Yalagi, J. Tonannavar and J. Tonannavar, *Heliyon*, **5**, e01933 (2019); https://doi.org/10.1016/j.heliyon.2019.e01933
12. M.D. Prabhu, J. Tonannavar (Yenagi), V. Kamat and J. Tonannavar, *J. Mol. Struct.*, **1218**, 128495 (2020); https://doi.org/10.1016/j.molstruc.2020.128495
13. S. Sarkhel and G.R. Desiraju, *Proteins*, **54**, 247 (2004); https://doi.org/10.1002/prot.10567
14. A. Jezierska, *J. Mol. Model.*, **21**, 47 (2015); https://doi.org/10.1007/s00894-015-2587-3
15. M.D. Prabhu, J. Tonannavar and J. Tonannavar, *J. Mol. Struct.*, **1246**, 131218 (2021); https://doi.org/10.1016/j.molstruc.2021.131218
16. P. Ramanna, J. Tonannavar and J. Tonannavar, *J. Mol. Struct.*, **1241**, 130613 (2021); https://doi.org/10.1016/j.molstruc.2021.130613
17. S.S. Malaganvi, J. Tonannavar (Yenagi) and J. Tonannavar, *J. Mol. Struct.*, **1181**, 71 (2019); https://doi.org/10.1016/j.molstruc.2018.12.063
18. L. Pallavi, J. Tonannavar and J. Tonannavar, *J. Mol. Struct.*, **1211**, 128085 (2020); https://doi.org/10.1016/j.molstruc.2020.128085
19. M.J. Frisch, G.W. Trucks, H.B. Schlegel, G.E. Scuseria, M.A. Robb, J.R. Cheeseman, G. Scalmani, V. Barone, B. Mennucci, G.A. Petersson, H. Nakatsuji, M. Caricato, X. Li, H.P. Hratchian, A.F. Izmaylov, J. Bloino, G. Zheng, J.L. Sonnenberg, M. Hada, M. Ehara, K. Toyota, R. Fukuda, J. Hasegawa, M. Ishida, T. Nakajima, Y. Honda, O. Kitao, H. Nakai, T. Vreven, J.A. Montgomery Jr., J.E. Peralta, F. Ogliaro, M. Bearpark, J.J. Heyd, E. Brothers, K.N. Kudin, V.N. Staroverov, R. Kobayashi, J. Normand, K. Raghavachari, A. Rendell, J.C. Burant, S.S. Iyengar, J. Tomasi, M. Cossi, N. Rega, J.M. Millam, M. Klene, J.E. Knox, J.B. Cross, R.L. Martin, V. Bakken, J.A. Jaramillo, R. Gomperts, R.E. Stratmann, O. Yazyev, A.J. Austin, R. Cammi, C. Pomelli, J.W. Ochterski, K. Morokuma, V.G. Zakrzewski, G.A. Voth, P. Salvador, J.J. Dannenberg, S. Dapprich, A.D. Daniels, Ö. Farkas, J.B. Foresman, J.V. Ortiz, J. Cioslowski and D.J. Fox, Gaussian 09, Revision D.01 Gaussian, Inc., Wallingford CT (2013).
20. R. Dennington, T. Keith and J. Millam, GaussView 5.0, Semichem Inc. Shawnee Mission, KS (2009).
21. V.A. Marenich, C.J. Cramer and D.G. Truhlar, *J. Phys. Chem. B*, **113**, 6378 (2009); https://doi.org/10.1021/jp810292n
22. J. Dziedzic, S.J. Fox, T. Fox, C.S. Tautermann and C.-K. Skylaris, *Int. J. Quantum Chem.*, **113**, 771 (2013); https://doi.org/10.1002/qua.24075
23. N.H. Rhys, A.K. Soper and L. Dougan, *J. Phys. Chem. B*, **116**, 13308 (2012); https://doi.org/10.1021/jp307442f
24. M.J. Abraham, D. van der Spoel, E. Lindahl and B. Hess, GROMACS Development Team, GROMACS User Manual version (2019).
25. H.J.C. Berendsen, D. van der Spoel and R. van Drunen, *Comput. Phys. Commun.*, **91**, 43 (1995); https://doi.org/10.1016/0010-4655(95)00042-E
26. D. Van Der Spoel, E. Lindahl, B. Hess, G. Groenhof, A.E. Mark and H.J.C. Berendsen, *J. Comput. Chem.*, **26**, 1701 (2005); https://doi.org/10.1002/jcc.20291
27. P. Szilard, M.J. Abraham, C. Kutzner, B. Hess and E. Lindahl, in eds.: S Markidis and E. Laure, Tackling Exascale Software Challenges in Molecular Dynamics Simulations with GROMACS; In: Solving Software Challenges for Exascale, EASC 2014, Lecture Notes in Computer Science, vol 8759. Springer, Cham. pp 3–27 (2015); https://doi.org/10.1007/978-3-319-15976-8_1
28. S. Pronk, S. Páll, R. Schulz, P. Larsson, P. Bjelkmar, R. Apostolov, M.R. Shirts, J.C. Smith, P.M. Kasson, D. Van Der Spoel, B. Hess and E. Lindahl, *Bioinformatics*, **29**, 845 (2013); https://doi.org/10.1093/bioinformatics/btt055
29. V.R. Kumar, C. Verma and S. Umapathy, *J. Chem. Phys.*, **144**, 064302 (2016); https://doi.org/10.1063/1.4941058
30. G. Bussi, D. Donadio and M. Parrinello, *J. Chem. Phys.*, **126**, 014101 (2007); https://doi.org/10.1063/1.2408420

31. W.G. Hoover, A.J.C. Ladd and B. Moran, *Phys. Rev. Lett.*, **48**, 1818 (1982); https://doi.org/10.1103/PhysRevLett.48.1818
32. U. Essmann, L. Perera, M.L. Berkowitz, T. Darden, H. Lee and L.G. Pedersen, *J. Chem. Phys.*, **103**, 8577 (1995); https://doi.org/10.1063/1.470117
33. B. Hess, C. Kutzner, D. Van Der Spoel and E. Lindahl, *J. Chem. Theory Comput.*, **4**, 435 (2008); https://doi.org/10.1021/ct700301q
34. W. Humphrey, A. Dalke and K. Schulten, *J. Mol. Graph.*, **14**, 22 (1996); https://doi.org/10.1016/0263-7855(96)00018-5
35. N. Choudhary, S. Bee, A. Gupta and P. Tandon, *Comput. Theor. Chem.*, **1016**, 8 (2013); https://doi.org/10.1016/j.comptc.2013.04.008
36. C.J. Cramer, Essential of Computational Chemistry Theories and Models, edn. 2, John Wiley & Sons (2004).
37. R. Chelli, R. Righini and S. Califano, *J. Phys. Chem. B*, **109**, 17006 (2005); https://doi.org/10.1021/jp051731u
38. S. Alavi, K. Shin and J.A. Ripmeester, *J. Chem. Eng. Data*, **60**, 389 (2015); https://doi.org/10.1021/je5006517
39. P.N. Patrone and T.W. Rosch, *J. Chem. Phys.*, **146**, 094107 (2017); https://doi.org/10.1063/1.4977516
40. U. Abdulkareem, T.R. Kartha and V. Madhurima, *J. Mol. Model.*, **29**, 151 (2023); https://doi.org/10.1007/s00894-023-05558-9
41. G.R. Desiraju and T. Steiner, The Weak Hydrogen Hond, Structural Chemistry and Biology, Oxford University Press (2001).
42. M. Arnittali, A.N. Rissanou and V. Harmandaris, *Procedia Comput. Sci.*, **156**, 69 (2019); https://doi.org/10.1016/j.procs.2019.08.181
43. P. Liu, J. Lu, H. Yu, N. Ren, F.E. Lockwood and Q.J. Wang, *J. Chem. Phys.*, **147**, 084904 (2017); https://doi.org/10.1063/1.4986552
44. N. Issaoui, H. Ghalla, S. Muthu, H.T. Flakus and B. Oujia, *Spectrochim. Acta A Mol. Biomol. Spectrosc.*, **136**, 1227 (2015); https://doi.org/10.1016/j.saa.2014.10.008
45. J.B. Foresman and A. Frisch, Exploring Chemistry with Electronic Structure Methods, edn. 3, Gaussian, Inc.: Wallingford, CT (2015).
46. S. Yalagi, J. Tonannavar and J. Yenagi, *Spectrochim. Acta A Mol. Biomol. Spectrosc.*, **181**, 109 (2017); https://doi.org/10.1016/j.saa.2017.03.041
47. L. Pallavi, Ph.D. Thesis, Spectroscopic MD and DFT Characterization of Some Phenylalanines, Department of Physics, Karnatak University, Dharwad, India (2022).
48. M.D. Prabhu, Ph.D. Thesis, Spectroscopic Study of Some Unnatural Amino Acids as Aided by DFT Modeling, Department of Physics, Karnatak University, Dharwad, India (2022).
49. J.P. Merrick, D. Moran and L. Radom, *J. Phys. Chem. A*, **111**, 11683 (2007); https://doi.org/10.1021/jp073974n
50. W. Liptay, *Angew. Chem. Int. Ed. Engl.*, **4**, 724 (1965); https://doi.org/10.1002/anie.196507241
51. L.J. Bellamy, The infra-red Spectra of Complex Molecules, Methuen and Co., London (1955).
52. G. Socrates, Infrared Characteristic Group Frequencies, John Wiley & Sons: New York, London, Sydney, Toronto (1980).
53. V.P. Nicu and E.J. Baerends, *Phys. Chem. Chem. Phys.*, **11**, 6107 (2009); https://doi.org/10.1039/b823558a
54. G. Longhi, M. Tommasini, S. Abbate and P.L. Polavarapu, *Chem. Phys. Lett.*, **639**, 320 (2015); https://doi.org/10.1016/j.cplett.2015.09.043
55. L.A. Nafie, Vibrational Optical Activity: Principles and Applications, Wiley (2011).
56. S. Gobi, E. Vass, G. Magyarfalvi and G. Tarczay, *Phys. Chem. Chem. Phys.*, **13**, 13972 (2011); https://doi.org/10.1039/c1cp20797k
57. E.D. Glendening, C.R. Landis and F. Weinhold, *Wiley Interdiscip. Rev. Comput. Mol. Sci.*, **2**, 1 (2012); https://doi.org/10.1002/wcms.51
58. A.E. Reed, L.A. Curtiss and F. Weinhold, *Chem. Rev.*, **88**, 899 (1988); https://doi.org/10.1021/cr00088a005
59. A.G. Petrovic, N. Berova and J.L. Alonso-Gómez, in eds.: M.-M. Cid and J. Bravo, Absolute Configuration and Conformational Analysis of Chiral Compounds *via* Experimental and Theoretical Prediction of Chiroptical Properties: ORD, ECD, and VCD, In: Structure Elucidation in Organic Chemistry: The Search for the Right Tools, Wiley-VCH Verlag GmbH & Co. KGaA, Chap. 5, pp. 65-104 (2015).
60. Y. Geng, L. Li, C. Wu, Y. Chi, Z. Li, W. Xu and T. Sun, *Molecules*, **21**, 875 (2016); https://doi.org/10.3390/molecules21070875
61. R. Ding, J. Ying and Y. Zhao, *R. Soc. Open Sci.*, **8**, 201963 (2021); https://doi.org/10.1098/rsos.201963
62. G. Pescitelli and T. Bruhn, *Chirality*, **28**, 466 (2016); https://doi.org/10.1002/chir.22600
63. D.A. Skoog, F.J. Holler and S.R. Crouch, Principles of Instrumental Analysis, Cengage Learning, edn. 7 (2016).
64. F. Kaneko, K. Yagi-Watanabe, M. Tanaka and K. Nakagawa, *J. Phys. Soc. Jpn.*, **78**, 013001 (2009); https://doi.org/10.1143/JPSJ.78.013001